PART II

PROPAGATION AND COMMUNICATION ISSUES FOR BIOMEDICAL TELEMETRY

6

NUMERICAL AND EXPERIMENTAL TECHNIQUES FOR BODY AREA ELECTROMAGNETICS

ASIMINA KIOURTI AND KONSTANTINA S. NIKITA

School of Electrical and Computer Engineering, National Technical University of Athens, Athens, Greece

6.1 INTRODUCTION

Recently, there is growing research activity on biomedical telemetry systems, while millions of people worldwide depend upon wearable, ingestible, and implantable biotelemetry devices to support and improve their quality of life. Such devices can be used to perform several monitoring, diagnostic, therapeutic, and interventional applications that range from cardiac pacemakers and defibrillators to emerging applications in visual prosthesis, brain computer interfaces, and monitoring of a variety of physiological parameters such as oxygen, glucose, pH level, pressure, and temperature.

Biotelemetry communication links are formed between biomedical devices placed on, inside, or in close proximity to the body and control/monitoring equipment placed at a short distance. Such links serve a variety of purposes including transmission of real-time or stored data and device parameter adjustment, with new opportunities constantly arising. Depending on the application scenario and performance requirements, biotelemetry links can be implemented in a number of ways:

- Inductive links formed between mutually coupled coils have widely been employed for data and power transcutaneous biomedical telemetry. The degree

Handbook of Biomedical Telemetry, First Edition. Edited by Konstantina S. Nikita.

of coupling is described in terms of the coils' mutual inductance, which indicates the proportion of the exterior (implanted) coil's field that is captured by the implanted (exterior) coil. However, low data rates as well as size, weight, and biocompatibility issues often prohibit the use of inductive biotelemetry. Inductive links for biomedical telemetry applications will be analyzed in Chapter 7.

- Wireless biotelemetry performed by means of antennas operating in predefined frequency bands can be used instead. Nowadays, design of wearable, implantable, and ingestible antennas is attracting high scientific interest to deal with challenges related to miniaturization, biocompatibility, and high-quality performance. Biomedical telemetry performed by means of antennas will be described in Chapter 8.
- The use of the human body itself as a transmission medium for electrical signals, known as intrabody communication, is recently serving as a data communication technique in biomedical telemetry. Transmission of low-power electrical signals through the human body, performed by means of either galvanic or capacitive coupling, is a promising approach for wireless intrabody data transmission between sensors. Intrabody communications will be discussed in Chapter 9.
- Finally, in order to answer many new demands for biotelemetry and to overcome various problems of radio telemetry, a technological method called optical biotelemetry has also been developed. Using light as a transmission medium, the bandwidth for signal transmission is greatly increased and many electromagnetic interference (EMI) problems can be solved. Realization of optical biotelemetry will be discussed in Chapter 10.

Non-ionizing EM fields in the RF and microwave (MW) regions of the EM spectrum have a strong potential in biomedical telemetry because of their ability to be transmitted, guided, and focused. As a result, significant scientific research has been reported and is currently being performed on diagnostic and therapeutic applications of EM fields in biotelemetry, including data and power transmission as well as induction or collection of biological responses.

The human body is an important part of the wireless biotelemetry channel. Propagation of EM fields inside and around the human body has been found to be highly complex and is strongly affected by a number of factors including the lossy, subject-dependant dielectric human tissues, and the geometry of the subject. Human subjects can be modeled either numerically (numerical models imported in numerical EM codes) or physically (physical models made from liquid, gel, or solid materials). In order to understand the basic ways in which EM waves interact with the body and, thus, identify optimal biotelemetry solutions, it is essential to study the EM properties of human tissues and (numerically or physically) model the body in a practical and realistic way.

Due to the risk of adverse health effects caused by the use of wireless biomedical telemetry devices adjacent to or implanted inside the human body, such studies are also significant toward minimizing interaction of these devices with biological tissues and preserving patient safety. Concerns and safety guidelines for unintended effects of fields induced by biomedical telemetry on the human body will be discussed in Chapter 11.

This chapter discusses the electrical properties of human tissues, as well as numerical and physical modeling of the human body, and corresponding numerical and experimental procedures. A brief outline of safety issues and conformance to (national and international) safety guidelines will also be presented.

6.2 ELECTRICAL PROPERTIES OF HUMAN BODY TISSUES

The human body is a heterogeneous medium consisting of several types of tissues (e.g., skin, muscle, fat, blood, and organs such as lung, liver, or heart). Human tissues contain insulating materials (lipids) and electrical charges (ions, electrically polarized molecules, etc.). Therefore, they can be viewed as a weakly conducting medium (dielectric).

Electrical properties of each type of tissue result from the interaction between the incident EM radiation and the tissue constituents at the cellular and molecular level and control the propagation, attenuation, reflection, and other behavior of EM fields inside and outside the human body. As a result, it is essential to know the dielectric properties of the lossy human tissues in order to understand the interaction of EM waves with the human body and enable a detailed analysis of RF transmission and absorption in biomedical telemetry systems.

Energy exchange in biological tissues occurs in terms of either free charges or dipolar molecules (e.g., water). When a temporal-variant EM field is applied, free charges are accelerated to produce current, resulting in resistive losses that depend on the conductivity of the tissue, while dipolar molecules are re-oriented accordingly (dipolar polarization). Adjustment is reached after a certain period of time, which is known as the relaxation time. The impact on the overall field strength is expressed in terms of the complex permittivity:

$$\varepsilon = \varepsilon_0 \varepsilon_r \tag{6.1}$$

where ε_0 is the permittivity of free space, and ε_r is the complex relative permittivity, defined as

$$\varepsilon_r = \varepsilon_r' - j\varepsilon_r'' \tag{6.2}$$

In equation (6.2), ε_r' is the relative permittivity of the material, and $\varepsilon_r'' = \sigma/\omega\varepsilon_0$ is the out-of-phase loss factor, where ω denotes the angular frequency of the EM field and σ the conductivity of the material.

In general, relative permittivity describes how the material is affected by electric fields, while conductivity describes attenuation of the EM wave as it transits the material. The loss tangent, defined as

$$\tan\delta = \frac{\varepsilon_r''}{\varepsilon_r'} \tag{6.3}$$

tells which component of the electrical properties dominates the effect on the field. At low frequencies, conductivity dominates the behavior of the field, while at high frequencies, the relative permittivity tends to dominate.

Based on equations (6.1) and (6.2), the complex permittivity of the lossy body tissues can, thus, be calculated as

$$\varepsilon = \varepsilon_0 \varepsilon_r' - j\frac{\sigma}{\omega} \tag{6.4}$$

Electrical properties of the human body are usually specified either in terms of ε_r' and ε_r'' or in terms of ε_r' and σ, as a function of frequency.

However, human tissues are heterogeneous dielectric materials and there exist several relaxation times. Relative permittivity and conductivity are a strong function of tissue type and frequency, with each tissue having a different frequency variation, as follows:

- Tissues with high water content (e.g., muscle, skin, or brain) feature higher permittivity and conductivity values than tissues with low water content (e.g., fat or bone) and are therefore more lossy. This behavior can be attributed to the resonant polar properties of water molecules.
- Relative permittivity decreases with frequency in three main steps known as the α, β, and γ dispersion regions, from values in the range of 10^5 at a few hundred hertz to less than 1 in the gigahertz range. Conductivity increases with frequency starting around 10^{-4} to above 1 in the same frequency range.

For example, Figure 6.1 shows relative permittivity data of two very extreme tissues, muscle and fat, in a range of frequencies. Conductivity values are presented in Figure 6.2. Results are obtained from a compilation presented by Gabriel et al. (1996), which covers several body tissues and provides values of the electrical properties at various frequencies.

High-order terms are necessary to mathematically describe the complex permittivity, and a model based on the summation of four Cole–Cole expressions is most

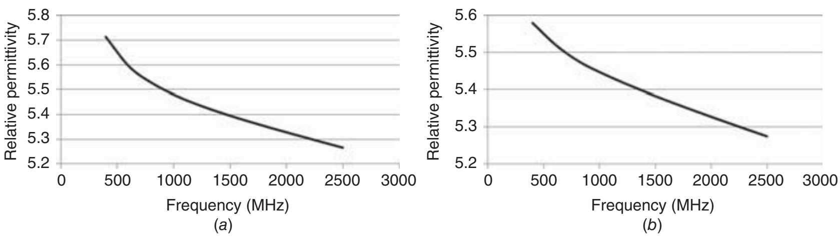

Figure 6.1 Dielectric permittivity values of (*a*) muscle and (*b*) fat tissues with respect to frequency.

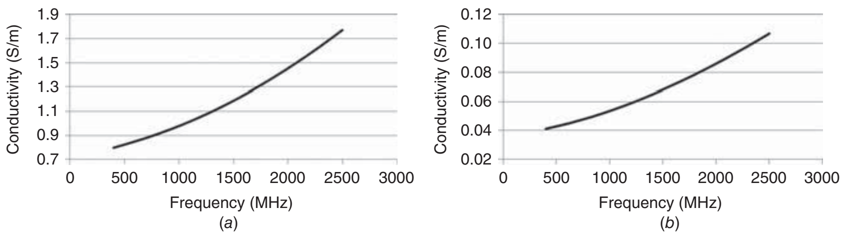

Figure 6.2 Conductivity values of (*a*) muscle and (*b*) fat tissues with respect to frequency.

commonly used (Gabriel et al., 1996):

$$\varepsilon = \varepsilon_\infty + \sum_{m=1}^{4} \frac{\Delta\varepsilon_m}{1 + (j\omega\tau_m)^{(1-a_m)}} + \frac{\sigma_j}{j\omega\varepsilon_0} \tag{6.5}$$

where ε_∞ is the material permittivity at very high frequencies (of the order of terahertz), ε_0 is the permittivity of free space, σ_j is the conductivity, and ε_m, τ_m, α_m are material parameters for each dispersion region.

Finally, an important parameter toward understanding EM propagation in human tissues is the skin depth, δ. The skin depth is a measure of the distance over which the electric field has been attenuated by a factor of $^1\!/_e$ or 0.368 from its original value and is defined as

$$\delta = \frac{1}{\alpha} \tag{6.6}$$

where a is the attenuation constant obtained from the real part of the propagation constant, γ, as

$$\gamma = \alpha + j\beta = j\omega\sqrt{\mu\varepsilon}\left(1 + \frac{\sigma}{j\omega\varepsilon}\right)^{1/2} \tag{6.7}$$

where μ is the permeability of the material.

At low frequencies, where relative permittivity values are high and conductivity values low, skin depth is significant and the EM wave can penetrate well into the human body. For example, at 433 MHz, 69% of the field is transferred through 10 cm of fat, and 11% is transferred through 10 cm of muscle. In implantable biomedical telemetry devices, the use of lower operation frequencies (e.g., 402 or 433 MHz) is, therefore, recommended. On the other hand, penetration of incident EM fields into biological tissues decreases with frequency. At high frequencies, conductivity values become high, skin depth decreases, and propagation is limited around the surface of the body. For example, at 2.45 GHz, the penetration depth is limited to 113 and 21 mm for fat and muscle, respectively.

Currently, the most comprehensive, complete, and best known database of electrical properties of body tissues is based on the work of Gabriel et al. (1996). Before this work was published, most data on the dielectric properties of tissues were obtained from measurements of animals, such as pigs, sheep, or rabbits. Based on these measurements, a Cole–Cole analysis was performed to propose a parametric model for several body tissues in a wide frequency range (from 10 Hz to 20 GHz).

It is worth noting, however, that significant deviations are observed to these commonly used values from data produced by other works (Smith and Foster, 1985; Campbell and Land, 1992). Smith and Foster measured the complex permittivities of two low-water-content tissues, bone marrow and adipose tissue, between 1 kHz and 1 GHz. Comparison with previous measurements of dielectric properties for high-water-content tissues suggested that bone marrow and adipose tissues contain less motionally altered water per unit dry volume compared with the previously studied tissues with lower lipid fractions (Smith and Foster, 1985). Campbell and Land (1992) measured the dielectric properties of female breast tissues at 3.2 GHz and concluded that apart from the dielectric relaxation of tissue water, dielectric relaxation of bound water and the tail end of a beta dispersion also affect the complex pemittivities at this frequency.

Several other research efforts have been performed to assess the electrical properties of human tissues. Recently, Lazebnik et al. (2007) reported the results of a large-scale, multi-institutional study characterizing the dielectric properties of normal breast tissue samples obtained from reduction surgeries at the University of Wisconsin and University of Calgary hospitals. The analysis of 354 tissue samples revealed that there was a large variation in the dielectric properties of normal breast tissue due to substantial tissue heterogeneity. No statistically significant difference was observed between the within-patient and between-patient variability in the dielectric properties. Furthermore, O'Rourke et al. (2007) characterized electrical properties of in vivo and ex vivo human liver tissues between 0.5 and 20 GHz. It was observed that wideband dielectric properties of in vivo liver tissue are different from the wideband dielectric properties of ex vivo liver tissue, and that the in vivo data cannot be represented in terms of a Cole–Cole model.

Variability of electrical properties has also been studied. Bao et al. (1997) presented in vitro complex dielectric measurements of gray and white matter of rat brain tissue in the frequency range between 45 MHz and 26.5 GHz. Two empirical models were suggested to describe the experimental data: the first model contained two Cole–Cole functions, while the second utilized one Havriliak–Negami and one Cole–Cole function. Standard deviations of the order of ± 4 to $\pm 16\%$ were reported (Bao et al., 1997). Electrical properties of animal tissues as a function of time after death have also been investigated (Schmid et al., 2003). Experiments were performed on pigs to investigate possible postmortem changes of the dielectric properties of brain gray matter in the frequency range of 800–1900 MHz. After being kept in stable anaesthesia for at least 45 min, animals were euthanatized, and measurements of dielectric properties were repeatedly performed from at least 45 min prior to death to 18 hr after euthanasia. A decrease by 4% in relative permittivity and by 10% in conductivity was observed in pig tissue 4 h after death. Results indicate that in vitro measurements of dielectric properties of brain tissue underestimate equivalent conductivity as well as permittivity of living tissue.

Furthermore, tissue electrical properties have been demonstrated to decrease with age for most tissues, as attributed to changes in water content and organic composition of the tissues. The dielectric properties of rat tissues at different ages have been measured (Peyman et al., 2001). Higher conductivity values were found for the brain and skull of newborn rats compared to adult rats at 900 MHz (16 versus 43%, respectively), while a lower increase of relative permittivity was also recorded (9.9 versus 33%, respectively). A significant dependence of the electrical properties of white matter and spinal cord on age has also been reported, while no age-related variation has been found for the gray matter (Peyman et al., 2007). Finally, a systematic evaluation of the age-dependent changes of the electrical properties of a large number of different tissues has recently been published (Peyman et al., 2009). In vitro dielectric properties of aging porcine tissues were measured in the frequency range of 50 MHz–20 GHz, and a statistically significant reduction with age in both permittivity and conductivity of 10 out of 15 measured tissues was observed. The establishment of a database for children's dielectric properties should be an essential and urgent task.

6.3 NUMERICAL MODELING

Numerical modeling provides an effective way of assessing and predicting the EM performance of biomedical telemetry systems in terms of radiation, propagation, and interaction with body tissues. Numerical modeling overcomes the inherent difficulties of experimental measurements and is considered of utmost importance in the calculation of field values inside body tissues as well as in the evaluation of implantable biomedical devices where it is impossible to make measurements in real operating scenarios.

Analytical methods can be applied to simplified canonical geometries modeling the human body (or parts of it), while numerical methods use body models ranging from very simple homogeneous models to millimeter resolution anatomic models, with the latter providing highly accurate results. Developing powerful, reliable, and subject-specific (in)homogeneous numerical phantoms is highly significant in reliably predicting the EM performance of biomedical telemetry systems.

6.3.1 Numerical Phantoms

Canonical Models Simple-shaped numerical phantoms, in the shape of a sphere or cube, are known as canonical models. These can be solved either numerically to provide an understanding of the exhibited EM performance through simplified estimations, or analytically for computer code checking.

Canonical models are computationally efficient with standard simulation resources and seem to be adequate for obtaining preliminary results. Inaccuracy comes from inaccuracy in modeling and not inaccuracy in the calculations. Furthermore, the choice of simple models provides the possibility to easily construct experimental phantoms complying with the numerical ones, which is important for validation purposes.

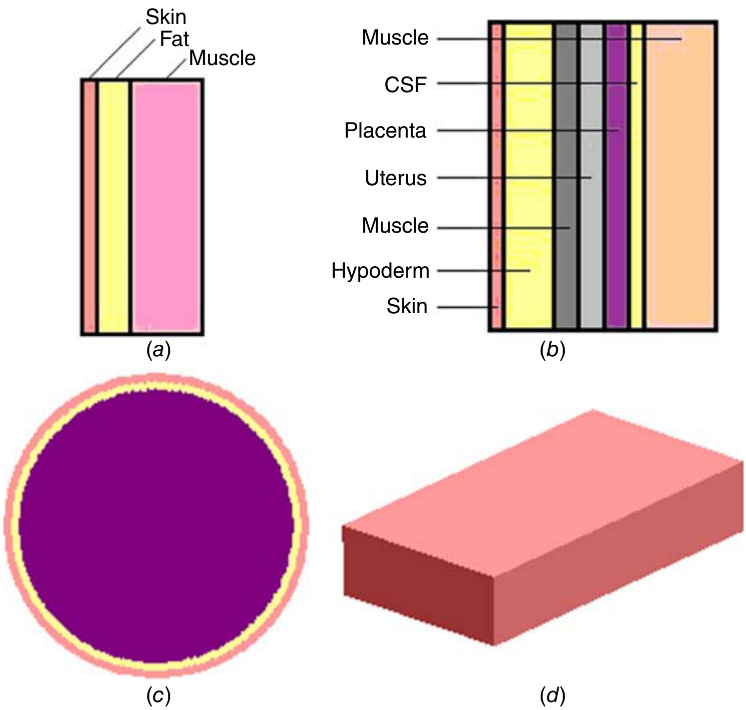

Figure 6.3 Whole-body canonical models used in (*a*) (Curto and Ammann, 2007) and (*b*) (Wiart et al., 2005), and canonical geometries modeling the human (*c*) head (Koulouridis and Nikita, 2004) and (*d*) torso (Kuhn et al., 2009).

Whole-body canonical models have largely been used in the literature to model the human body. A planar three-layer body model, consisting of a low-water-content tissue layer (fat) embedded between two high-water-content tissues (skin and muscle) has been proposed (Curto and Ammann, 2007) (Figure 6.3*a*). The study reported on the coupling mechanism of a half-wavelength dipole at 434 MHz, as a preliminary step toward analyzing antennas interacting with tissues in the near and farfields. Nine combinations of skin, fat, and muscle tissue with different thicknesses were analyzed to model the absorption in different parts of the body. A multi-layer structure composed of skin, hypoderm, muscle, uterus, placenta, amniotic fluid (considered as cerebrospinal fluid, CSF), and fetus (considered as muscle) has also been analyzed (Wiart et al., 2005) (Figure 6.3*b*). The study assessed the main parameters influencing the RF exposure of children's heads. The evolution of the head shape and the growth of specific parameters, such as the skull thickness, were taken into account and comparisons with corresponding results in adults were reported. Cylindrical phantoms can otherwise be applied for whole-body models.

Canonical geometries have also been used to model specific parts of the human body. For example, a three-layer spherical human head model consisting of skin, bone, and brain tissues has been used (Koulouridis and Nikita, 2004) (Figure 6.3*c*).

The aim was to study the interaction between normal-mode helical antennas and human head models, while emphasizing the comparative dosimetric assessment between adults and children head models. Rough approximations of the human head have also been obtained by using homogeneous or layered dielectric box models. Furthermore, a rectangular structure filled with tissue-emulating material has been used to model the human torso (Kuhn et al., 2009) (Figure 6.3*d*). The study evaluated the radiation emitted by mobile phones when used with wireless and wired hands-free kits in order to assess the significance of a dedicated compliance procedure and the extent to which the use of wired and wireless hands-free kits can reduce human exposure.

Regarding children models, it is most commonly assumed that a child model is perfectly proportional to an adult model. As such, children canonical models are obtained through uniform downscaling of the corresponding adult models. For example, homogeneous and multi-layer spherical children head models have been obtained through uniform deformation of spherical adult head models (Koulouridis and Nikita, 2004).

Example canonical models used in recent biomedical telemetry studies are shown in Figure 6.4:

- A spherical six-layer head model consisting of brain, CSF, dura, bone, fat, and skin has been used to characterize a dipole antenna implanted inside the human head and operating at the biomedical frequency band of 402–405 MHz (Figure 6.4*a*) (Kim and Rahmat-Samii, 2004). The human head was simplified as a lossy multi-layered sphere to allow analytical solving of the EM problem and facilitate parametric studies.

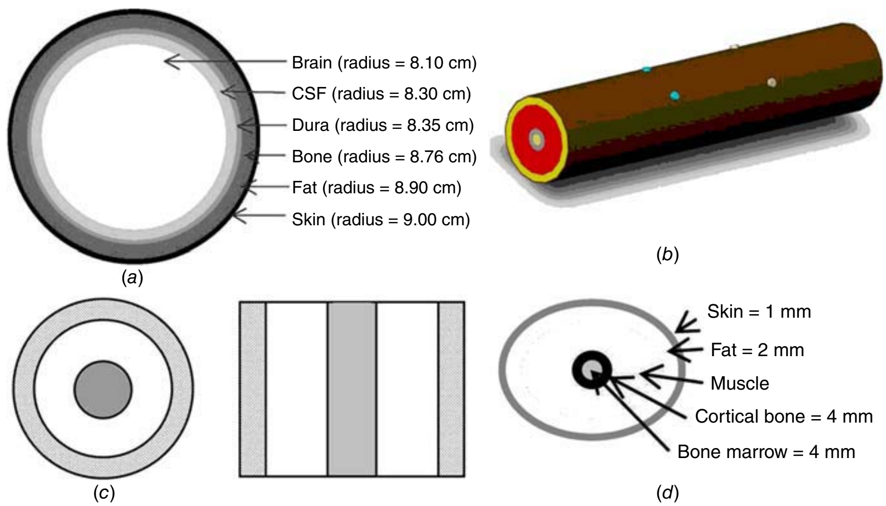

Figure 6.4 Canonical phantom models used to model the human (*a*) head (Kim and Rahmat; Samii, 2004), (*b*) upper arm (Wegmueller et al., 2007), (*c*) thigh (Weiss et al., 2009), and (*d*) arm (Lim et al., 2011) in recent biomedical telemetry studies.

- The geometry of the human upper arm has been modeled by concentric cylinders representing the skin, fat, muscle, cortical bone, and bone marrow layers in order to characterize it as a transmission medium for electrical current (galvanic coupling) (Figure 6.4*b*) (Wegmueller et al., 2007). Properties of specific types of tissue, as well as geometrical body variations were investigated, and different electrodes were compared.
- A thigh model consisting of concentric cylinders representing the bone, muscle, and fat has been presented to study the biotelemetry link for an artificial hip joint (Figure 6.4*c*) (Weiss et al., 2009). The accuracy of the cylindrically symmetrical model was verified through comparison of simulation results with measurements performed for a 433-MHz biomedical telemetry link in a 6-cm-thick porcine thigh.
- Finally, the human arm has been approximated as a conical frustum (tapered cone) of different radii and axis ratio as well as tissue compositions (single- or multiple-tissue layers and different thicknesses of tissue combinations) to report results on ultrawide-band (UWB) signal propagation along the human arm (Figure 6.4*d*) (Lim et al., 2011). The tissue types used included skin, fat, muscle, cortical bone, and bone marrow. The aim of this study was to assess the accuracy and efficiency and, thus, the suitability of such a simplified canonical model, as well as to investigate the effects of the model's structure complexity on the simulation results.

Anatomical Models To obtain more accurate simulation results, it is necessary to use realistically shaped numerical phantoms consisting of several types of tissues, known as anatomical models. The human body (or parts of it) is modeled by cubic cells (voxels) in which tissue electrical properties (relative permittivity and conductivity) are considered constant. By assigning the corresponding electrical properties to each voxel, one can easily model the anatomical tissues and organs.

Development of anatomical models is one of the most significant challenges in numerical bioelectromagnetics, and nowadays it is facilitated by the progress in medical imaging technologies and the increase in computing power. As computing power increases and computer resources get less expensive, there is a trend to refine the numerical description of the space modeled and move to more detailed anatomical structures. In contemporary models, the highest complexity used for modeling the whole human body is about 50 tissue types, and the finest resolution is about 1 mm. Advanced computer graphics techniques can be employed to pose such models in virtually any position.

In the majority of studies, the data for designing the anatomical body models are taken from magnetic resonance imaging (MRI) or computed tomography (CT) scans. MRI and CT scans provide gray-scale image data of the human body at several transverse slices at a designated spacing. The resolution in each slice is on the order of several millimeters. Several tissues can be distinguished; however, image segmentation is further required to convert the density mappings into tissue maps. This is generally a complex and time-consuming activity and is performed semi-manually, although automatic methods have been reported as well. Even if software for automatic identification is applied, manual verification or correction is required. MRI data are generally superior to CT data in identifying interior tissues because of the high contrast images of the soft tissues. It is worth noting that MRI or CT produced in different laboratories inevitably contain differing discretizations.

Furthermore, the resolution of the medical imaging techniques is, presently, too high for using their results directly in numerical modeling. Several anatomical models have been developed for use in a wide range of applications:

(a) Data acquired from CT scans of a cancer patient have been used to create a model consisting of approximately 35,000 10-mm-edge cubic cells (Sullivan, 1990). Simulations were conducted to assess the electric field distribution for various prototype applications used in deep regional hyperthermia, and comparison with measurements was performed to investigate the ability to simulate the patterns from the near field of the applicators.

(b) A whole-body model of 1.9 mm $\times$ 1.9 mm $\times$ 3 mm resolution based on MRI scans of an adult male (height 1.88 m, weight 64 kg), scaled to 71 kg, and segmented into 30 types of tissue has also been reported (Gandhi et al., 1996). The EM energy coupled to the head due to mobile phones operating at the frequencies of 835 and 1900 MHz was studied, and the effect of using simplified homogeneous models instead of the anatomical heterogeneous models was assessed.

(c) The Visible Human Project (VHP) (Ackerman, 1998) has made available a digital axial anatomical image library at 1-mm resolution of the body of a human male, named Hugo, based on data from a 38-year-old cadaver (height 1.86 m, weight 90 kg) (Figure 6.5*a*). This project involved the creation of complete, anatomically detailed, three-dimensional representations of the normal male and female human bodies, and its long-term goal was to produce a system of knowledge structures that would transparently link visual knowledge forms to symbolic knowledge formats such as the names of body parts. Hugo's body model is larger than that of an average male and

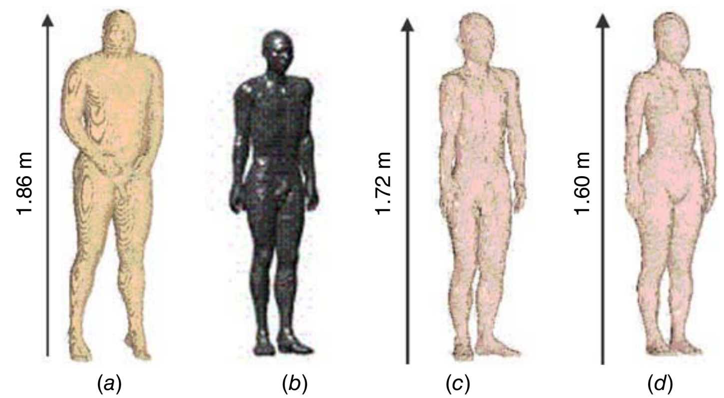

Figure 6.5 Anatomical models of (*a*) Hugo (Ackerman, 1998), (*b*) Norman (Dimbylow, 2002), (*c*) Japanese male (Nagaoka, 2004), and (*d*) Japanese female (Nagaoka, 2004).

consists of 38 tissues. Various studies have been performed with the VHP Man, and the model is nowadays being included in many commercially available EM simulation tools. Furthermore, the deviation of Hugo's dimensions (height and weight) from the average values has promoted development of other anatomically realistic models with average height and weight.

(d) The Norman model consists of 2-mm-edge cubic voxels based on MRI scans of a subject, scaled to the height and mass of a reference man, and segmented to 38 types of tissue (Dimbylow, 2002) (Figure 6.5b). The reduction in voxel size compared to previous works allowed dosimetric quantities to be calculated at higher frequencies, while calculations were extended down to 10 MHz to cover the whole-body resonance regions.

(e) Finally, two 2-mm-resolution whole-body Japanese models with hands placed at the side of the body have been developed using MRI (Nagaoka et al., 2004). These classified over 50 types of tissues and were based on images of a 22-year-old male (height 1.73 m, weight 65 kg) (Figure 6.5c) and a 22-year-old female (height 1.60 m, weight 53 kg) (Figure 6.5d). The reported female model was the first of its kind in the world, and both the male and female models were the first Asian voxel models (representing average Japanese), which enabled numerical evaluation of dosimetric quantities at frequencies of up to 3 GHz.

Due to the lack of children MRI or CT images, the first anatomical children models in the literature were based on uniform downscaling of adult models. However, the uniform downscaling approach does not take into account the different growth patterns of certain parts of the body. For example, head growth is age dependent. The volume of the brain, the skin, and skull thickness each grow at different rates. As a result, the scaled children models do not exactly reproduce the dimensions and anatomy of children. A more realistic approach suggests making a piecewise reduction of the adult model with respect to the main anatomical parameters. The adult model is divided in different parts and non-uniform downscaling is applied to each of these ("child-like" approach). However, inaccuracies in the size of the non-uniform downscaled child models are still present. As a result, recently, whole-body child models have been developed based on MRI or CT database of children. In Wiart et al., (2008), several MRI data sets of children at different ages from three different French hospitals were used to provide segmented versions of children head models. Six child head models at different ages (5, 6, 8, 9, 12, and 15 years old) were built using this approach, as illustrated in Figure 6.6.

Example anatomical models used in recent biomedical telemetry studies are shown in Figure 6.7. The 67-biological-tissue phantom file of a human body produced at Yale University (Zubal et al., 1994) has been translated into a 30-biological-tissue model to analyze the characteristics of a head-implantable dipole antenna (Figure 6.7*a*) (Kim and Rahmat-Samii, 2004). Implantable antennas have been analyzed inside a 31-tissue realistic model of the human shoulder derived from the University of Utah model (Figure 6.7*b*) (Soontornpipit et al., 2004), while an anatomical human head model comprising 24 biological tissues has been used to characterize the transmission of RF signals between implantable and free-space loop antennas (Figure 6.7*c*) (Chen et al., 2009). Finally, 2-mm-resolution human body models have been developed at

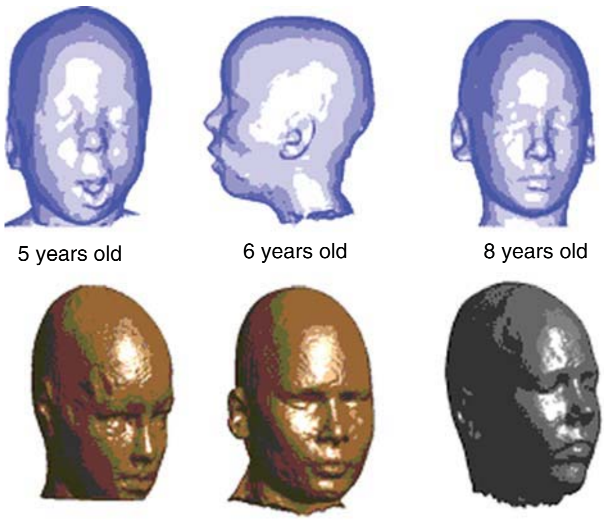

Figure 6.6 Child head models based on MRI data sets of children at different ages (Wiart et al., 2008).

different postures on the basis of average statistical values of the body parameters of Asian adults in order to investigate on-body UWB communication (Figure 6.7*d*) (Wang et al., 2009).

However, it is worth noting that even though heterogeneous models are more representative of actual coupling in human tissue, it has been observed that homogeneous models overestimate the absorbed energy and can be considered as worst-case approximations. This is why, although sophisticated body models have appeared in most recent studies, the homogeneous model case has almost always been present as well.

6.3.2 Computational Methods

Analytical Methods Analytical techniques are so called because, in contrast to numerical techniques, they consist of some solution to Maxwell's equation that is not based on a direct numerical solution and does not require the inversion of large matrices. Exact solutions to Maxwell's equations can be found in terms of mathematical formulas that describe the propagating EM fields. The main restriction consists in adopting a simplified canonical geometry for modeling the human body (or parts of it). The choice of such highly simplified geometries is essential due to the necessity of characterizing a structure resembling the human body (or parts of it) and having at the same time a closed form of the wave equation.

For example, body heating due to exposure to 150 MHz–10 GHz fields has been investigated by analyzing transmission and reflection at boundaries within

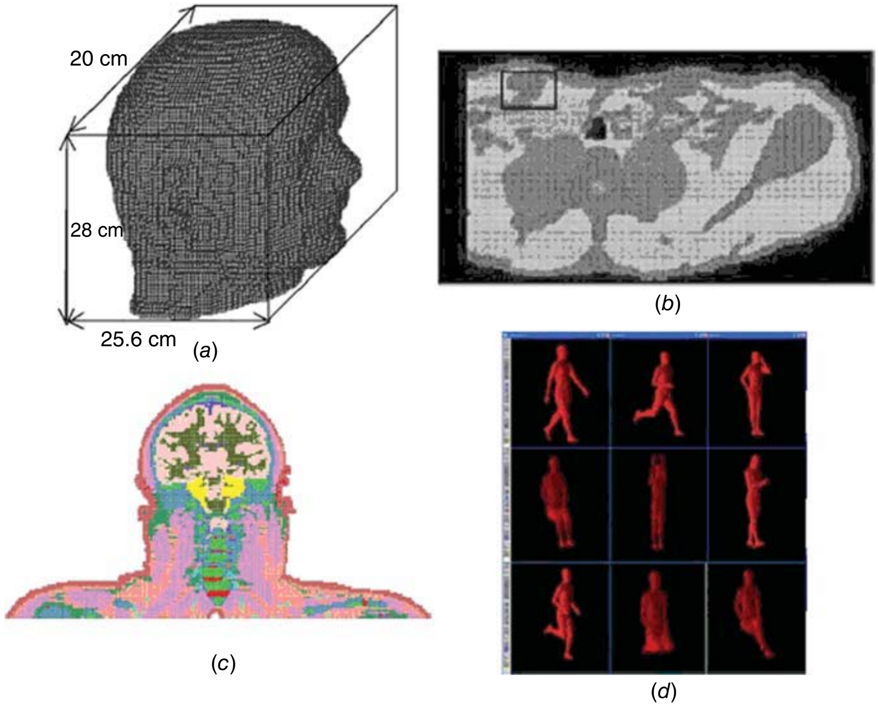

Figure 6.7 Anatomical phantom models used to model the human (*a*) head (Kim and Rahmat-Samii, 2004), (*b*) upper shoulder (Soontornpipit et al., 2004), (*c*) head with shoulders (Chen et al., 2009), and (*d*) body (Wang et al., 2009) in recent biomedical telemetry studies. (*See insert for color representation of c and d.*)

a three-layered (skin, fat, and muscle) planar model (Schwan and Li, 1956). Two quantities were considered to analyze EM radiation inside the human body and the resultant heat development: (a) the percentage of airborne EM energy absorbed by the body and (b) the distribution of heat sources in skin, subcutaneous fat, and deeper situated tissues. Analysis of the irradiation of spherical head models using spherical vector wavefunctions has also been reported (Weil, 1975). The head models consisted of a core of brain-like material surrounded by five outer layers of CSF, bone, fat, and skin-dura tissues, while their outer radii ranged in size from 2 to 12.5 cm. The distribution of internally deposited energy was also investigated for three basic spheres with radii of 3.3, 6, and 10 cm, to study the creation of hot spots (i.e., localized regions of strong heating).

The problem of interaction between a homogeneous sphere and a simple waveform (e.g., plane wave, short dipole, etc.) has been treated using analytical methods (Lin, 1976). The transmitted field strengths in homogeneous spherical models of human and animal heads were determined as a function of time and position using frequency analytic techniques. Constant conductivity was assumed for the electrical behavior of the brain matter. Zhou and Oosterom (1992) focused on the evaluation of the potential distribution inside spherical or spheroid volumes. A quasi-static approximation was used because of the low-frequency range of interest, but the method was applied to layered anisotropic media.

Nowadays, analytical methods are still used to find the exact solutions in simplified geometries and verify the accuracy of simulation results. For example, Kim and Sahmat-Ramii (2004) modeled the human head as a six-layer lossy dielectric sphere and implemented a spherical dyadic Green's function (DGF) code to characterize a dipole antenna implanted inside the human head. Gupta et al., (2008) used the DGF in a cylindrical human body model to obtain a simplified channel model. Four possible cases were considered, where the transmitter and receiver were either inside or outside the body, and an exact analytical expression was derived for the case where both the transmitter and receiver were placed out of the body.

Despite being restricted to very simple configurations, analytical methods significantly contribute to qualitative analyses. They are particularly useful to provide an insight into the physical mechanisms of EM propagation and interaction with biological tissues, identify the structure resonant frequencies that represent conditions of maximum power deposition inside the human body, evaluate the effect of dielectric and geometric parameters spread, and test the accuracy and performance of numerical codes.

Numerical Methods Numerical methods involve numerical solutions to Maxwell's equations subject to a set of initial or boundary values and are generally implemented on powerful computing platforms. They can handle complex geometries and provide a physical insight into the EM performance of the simulated systems. The constant evolution of computer systems (e.g., parallel systems) offers new possibilities for the execution of numerical codes with high computing requirements, thus facilitating more realistic and accurate modeling.

Several numerical techniques are available, with each using different forms of Maxwell's equations and employing different methods for their solution, thus each having its own advantages and drawbacks for particular applications. Among them, four have been most commonly used in bioelectromagnetics: the method of moments (MoM) (Harrington, 1968), the finite-element method (FEM) (Silvester and Ferrari, 1996), the finite-difference time-domain (FDTD) method (Yee, 1966), the transmission line matrix (TLM) method (Christopoulos, 1995), and the multiple-multipole (MMP) method (Hafner, 1990). Hybrid methods derived from the combination of these methods and other methods for EM propagation characterization are also used.

(a) Method of Moments The MoM was introduced by Harrington (1968) in a very general formulation. With this method, the problem is initially formulated in terms of integral equations obtained by using Green's functions. After appropriate choice of basis and weighting functions, these equations are reduced to a system of linear equations and solved.

The MoM is very efficient in modeling thin-wire structures and scattering from perfectly conducting objects. A significant advantage of this method is that only the structure in question (and not free-space) is discretized, thus limiting computational space, and boundary conditions do not have to be set.

On the other hand, the MoM is not effective for modeling arbitrarily shaped configurations, while memory requirements scale in proportion to the size of the problem, thus making EM characterization of physically and geometrically complex objects very difficult (or impossible) and time consuming. As a result, the MoM is not generally suitable for simulating the interactions between biomedical telemetry systems and the human body. The problem size grows so fast that the method does not allow a reasonably fine discretization of the human body. This also limits its application at frequencies higher than several hundred megahertz because smaller size blocks are required for higher frequencies.

Despite its drawbacks, MoM numerical solutions in bioelectromagnetics problems do appear in the literature. For example, Ito et al., (1992) and Chuang and Chen (1997) used the MoM to investigate the effect of the human body on small loop antennas in pager systems. Ito et al. (1992) approximated the human body as a conducting reflecting surface, for simplicity reasons. The influence of a reflector on the input impedance of a small loop antenna was examined both experimentally and theoretically, and results obtained by using the MoM were compared with experimental data to confirm the validity of the numerical method. Chuang and Chen (1997) adopted a crude squared model of the human body and assessed its effect on the performance of a circular-loop-wire antenna, which simulated the pager antenna. The MoM was employed to study the antenna characteristics and body absorption at 152, 280, and 400 MHz. More recently, Psychoudakis et al. (2008) considered a realistic homogeneous body model to analyze the performance of a body-worn diversity antenna for communications in the 225–380 MHz band. MoM techniques were employed to estimate optimum positioning and orientation for improved channel capacity, and results were validated through measurements for a human body phantom.

(b) Finite-Element Method The FEM was introduced in 1996 by Silvester and Ferrari (1996). It is based on the discretization, or, equivalently, meshing, of the EM problem into a number of elements of various shapes (usually tetrahedral) and sizes. Small elements are used to describe complex geometries, while larger elements are used in uniform regions.

The field equations are determined in terms of polynomials (interpolation functions) with unknown coefficients defined on the mesh nodes (corners of the elements) or along the element edges. In the edge-element technique the unknowns are associated with the fields that are tangential to the edges of the basic element. Within each element, vector expansion functions are used that are tangential to all element surfaces of which the edge is part and normal to all other surfaces. In contrast to the node-based FE technique, the edge-element technique possesses a direct way of controlling discretization errors in the solution by looking at the behavior of the normal components of the field between elements. Furthermore, the edge-element technique is more appropriate to model heterogeneous problems because there is no need to enforce any internal boundary conditions between elements with different electrical properties.

The major advantage of the FEM is that the electrical and geometric properties of each element can be defined independently. The FE mesh gives, in principle, very high flexibility in discretizing complicated geometries and is very efficient in modeling curved structures and arbitrarily shaped dielectric regions. As a result, the FEM has been widely used in bioelectromagnetics.

For example, Renhart et al. (1994) adopted the FEM to calculate eddy currents in the human body when magnetic resonance techniques were employed for diagnosis at the frequency of 64 MHz. A model was introduced that was feasible for FEM techniques without neglecting the most important organic influences on the eddy currents. The model was further analyzed, and the derived simulation results were compared with measurements obtained by MRI. Regarding functional electrical stimulation (FES), FEM models have frequently been used to find the parameters that have the biggest influence on nerve activation during stimulation. Kuhn and Keller (2006), used FE modeling combined with an active nerve model to assess the influence of the human anatomy and tissue properties on the electrical stimulation performance. Both the resistivity and permittivity of tissues were taken into account, and emphasis was given to the influence of muscle permittivity. Wegmueller et al. (2007) investigated the dependence of galvanic coupling on geometry and tissue parameters through FEM simulations with a mesh size of 150,000–200,000 elements. Simulation results showed that an increase in distance by 5 cm between transmitter and receiver increased the attenuation by 6–9 dB. Joints were found to increase the attenuation by up to 8 dB, with larger joints resulting in higher attenuation factors. Finally, Weiss et al. (2009) reported FE simulation results on the RF coupling of a 433 MHz near-field biotelemetry link for an artificial hip joint (titanium implant). Power losses were discussed as a function of patient size and antenna positioning, and accuracy of the simulation results was verified through experimental investigations in live porcine tissue.

The main drawback of the FEM is its relatively high computational complexity. Furthermore, the generation of meshes in three dimensions is a formidable task. While there are reasonably good techniques for the discretization of technical structures, the difficulty of generating FEMs for the typically very heterogeneous problems in dosimetry currently prevents wider use.

(c) Finite-Difference Time-Domain Method The FDTD is a powerful method for solving Maxwell's equations in three-dimensional space and time for the six-vector components of the electric and magnetic fields (Yee, 1966). Space is discretized in the form of cubic cells (dimensions of Δx, Δy, Δz), known as the Yee cells. Electric field (E) and magnetic field (H) components form the edges, and the normals to the faces of the cells, respectively, as shown in Figure 6.8. Simulation time is divided into time interval steps (Δt), and Maxwell's equations are solved iteratively in the cells as time is stepped forward. The electric and magnetic field components in the grid are updated in a leapfrog scheme using the finite-difference form of the curl operators on the fields that surround each component. The field updating process stops when the field quantities over the computational volume reach a steady state.

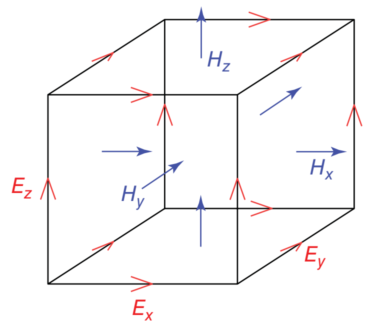

Figure 6.8 The Yee cell of the FDTD method.

The FDTD has the following main advantages:

- It is very versatile in analyzing complex geometries and can efficiently model arbitrary configurations of heterogeneous structures (e.g., the human body in various postures) with high spatial resolution.
- It demonstrates high computational efficiency because it requires only $O(N)$ computer complexity, where N is the number of the unknowns, and there is no need to invert large matrices. This means that the total memory storage required as well as the computational time are directly related to the number of field unknowns in the problem space (which in turn depends on the electrical size of the problem space and space resolution). For comparison, the MoM and the FEM need $O(N)^2$ computational storage.
- Because it is a time-domain technique, wideband results (i.e., results in a broad frequency range) can be obtained with a single simulation, simply by performing a fast Fourier transform on the time-domain response.
- There is no intrinsic upper bound to the number of unknowns it can solve.

On the other hand, the following points need to be carefully addressed in FDTD modeling:

- The entire computational domain has to be meshed. Cells must be smaller than the smallest wavelength divided by 10, and smaller than the smallest feature in the model. This greatly increases the number of cells for which calculations must be made, thus requiring a large amount of computer memory. In bioelectromagnetics, the smallest wavelength is generally found in the tissue with the highest water content at the highest frequency of interest.
- An upper bound on the time step (Δt) is required to ensure stability. Stability issues have thoroughly been discussed in Taflove and Hagness (2000). Once the cell size has been selected, the maximum time step is determined by the Courant

stability condition, which leads to a final upper bound given by

$$\Delta t \leq \left(c\sqrt{\frac{1}{(1/\Delta x)^2 + (1/\Delta y)^2 + (1/\Delta z)^2}} \right)^{-1} \tag{6.8}$$

- A very fine, dense, grid (and, therefore, a small time step) is required in modeling curved structures, sharp edges, or small geometric features, which in turn drastically increases computational time and memory required. Although non-uniform meshing and sub-gridding techniques can be applied, they may result in spurious solutions or suffer from instability (Monk and Suli, 1994).
- Difficulties may be encountered in modeling antenna structures not conforming to the used grid, such as helical antennas (Cavagnaro and Pisa, 1996; Nikita et al., 2000).

Nevertheless, the FDTD is being considered as the most suitable technique for modeling EM wave propagation inside and around the human body and is, currently, the most prevalent computational method in bioelectromagnetics. This is due to the fact that enhanced computer power has become available at lower cost, while intensive research work in the fields of source modeling, absorbing boundary conditions, and error checking has facilitated simulations with more confidence in the obtained results. The body model is discretized into Yee cells, and electrical properties are assigned to each cell to model human tissues before calculating the electric and magnetic fields as a function of time.

One of the first studies is that of Sullivan et al. (1987), who showed the capacity of the FDTD to compute EM energy absorption in human tissues. The FDTD method was evaluated by comparing its results to analytic solutions in two and three dimensions. The results obtained demonstrated that the FDTD method is capable of calculating internal dosimetric quantities with high accuracy. Since the early 1990s, the FDTD has been widely applied to the study of safety issues in mobile communications.

Regarding biomedical telemetry applications, the FDTD has more recently been used to study the radiation from implantable devices and evaluate the behavior of body-worn antennas. Chen et al. (2009) carried out FDTD investigations to characterize the transmission of RF signals between loop antennas placed in free space and implanted under the skull. The study assessed the effects of the human head on the transmission of RF signals between the implanted and exterior antennas, and simulation results were verified through measurements with a phantom. Computational models based on the FDTD were developed in Zhao et al. (2006) and Wang et al. (2009), with a single-cell Hertzian dipole being used as the excitation source, with the aim to provide a physical insight of the on-body radio channel. More specifically, Zhao et al. (2006) presented modeling for the ultrawideband on-body radio channel, and divided the frequency band between 3 and 9 GHz into 12 sub-bands to take into account the material frequency dispersion. Each subband was simulated separately, and a combination technique was subsequently employed (Zhao et al., 2006).

Wang et al. (2009) modeled on-body channels by simulating various body postures. Based on the FDTD simulation results, an on-body propagation model was derived and the model parameters for some representative transmission links on the human body were determined. Experimental measurements were performed to verify the simulation results for the chest-to-right-waist transmission link, and model parameters were found to highly agree between the two approaches (Wang et al., 2009). Finally, Kiourti et al. used the FDTD to study the resonance, radiation, and safety performance of a miniature antenna intended for integration in wireless head-implantable biomedical telemetry devices (Kiourti and Nikita, 2012, 2013; Kiourti et al., 2012).

(d) Transmission Line Matrix Method The TLM method provides discretization in both time and space (Christopoulos, 1995). Unlike other time-domain numerical methods, which are based on the direct discretization of Maxwell's equations, the TLM embodies Huygen's principle in discretized form. The method is based on the analogy between the electromagnetic field and a mesh of transmission lines, and, thus, considers the computational domain as a mesh of transmission lines, interconnected at nodes. Electric and magnetic fields are made equivalent to voltages and currents on the network, respectively. The mesh is initially excited by voltage impulses at specific points, which further propagate into the mesh while bouncing at the boundaries and being scattered by the nodes.

The TLM has proven to be one of the most powerful time-domain methods, especially for the computation of complex three-dimensional electromagnetic structures. Recently, this numerical method is being applied in the field of biomedical telemetry to assess the performance of advanced wearable liquid antennas, that is, antennas that are based on engineering the properties of liquids to communicate information about a person's health condition (body temperature, tissue damage, tumors, inflammation, and breathing). For example, in Traille et al. (2008) a bracelet-type liquid antenna consisting of an aqueous salt solution ($\varepsilon_r = 38$) inside a very thin plastic tubing container was characterized through numerous TLM calculations.

(e) Multiple-Multipole Method The MMP method is based on the generalized multipole technique (GMT) in which the fields are expanded as a linear superposition of basis functions (Hafner, 1990). As the name of the method suggests, the multipolar functions are the most used basis functions. These are obtained from the Helmholtz equation by separation of variables in spherical coordinates. The region where the fields are to be computed is divided into domains in which the material parameters are constant. The electric and magnetic fields are expanded as a linear superposition of known analytical solutions and are computed by minimizing the errors in the fulfillment of the boundary conditions.

The MMP method offers a high degree of freedom in the selection of the multipole basis functions, thus providing a high degree of accuracy. Furthermore, it offers the possibility of estimating the quality of the solution found, through evaluating the residual errors at the interfaces of the domains. Because of its efficiency, accuracy, and validation capability, the MMP method is especially suited to handle high-gradient fields in the vicinity of biological bodies. On the other hand, positioning of the multipolar function origins is difficult, giving rise to the development of several procedures for locating the multipoles (or auxiliary sources) in a systematic way. Moreover, MMP shows strong limitations for scatterers with complicated angular shapes or inhomogeneous bodies. In these cases, modeling of only the homogeneities that are of interest is generally preferred.

(f) Hybrid Methods Based on the above, none of the numerical methods and commercially available codes seems to be completely satisfactory for all cases of interest. A way to overcome the problems and drawbacks specific to each method is to use hybrid techniques. Combining existing methods into new hybrid approaches allows for highly efficient and robust numerical methods for application-specific scenarios, while keeping all the advantages and eliminating the disadvantages of component methods.

For example, a hybrid FEM/MoM method was employed by Meyer et al. (2003) to evaluate safety issues in the near field of a GSM base station antenna. The FEM was used to model the human phantom, while the MoM was used to model the metallic surfaces and wires of the antenna. The mathematical formulation of the hybrid technique was presented, and a discussion was performed on implementation details. The performance of the proposed hybrid FEM/MoM method was further validated by comparing results to MoM and FDTD solutions of human exposure problems.

Another typical hybrid technique is the combination of the MoM and the FDTD method. The method permits the computationally efficient FDTD method to model dielectrics, and the MoM, which represents conducting structures more accurately, to model antenna structures. It is, thus, particularly useful for analyzing complex problems that involve coupling between antennas and dielectric volumes (e.g., the human body). A hybrid FDTD/MoM technique was used by Chen et al. (1998) and Abd-Alhameed et al. (2005) to assess safety due to exposure to the radiation of an MRI transmit coil and base station antennas operating at 1800 MHz, respectively. Chen et al. (1998) computed the EM fields of shielded RF coils loaded with an anatomically human head model for high-frequency MRI applications and found that the proposed hybrid technique could accurately predict dosimetric quantitites excited by the RF coils. Finally, Abd-Alhameed et al. (2005) used a hybrid FDTD/MoM technique to verify the compliance of safety standards for mobile communications base stations and compared its performance with the traditional power density method.

(g) Boundary Conditions Most EM problems entail a structure whose behavior is to be studied in an infinite unbounded computational space. Because of the limited computer resources, infinite geometries cannot be simulated, and, thus, a method of terminating the computation domain is required. This is achieved by adding absorbing boundary conditions (ABCs) at the outside of the simulation space, which effectively simulate unbounded regions (infinite space) by minimizing reflections in the boundaries.

ABCs can be achieved in a number of ways. For example, Engquist and Majda (1977) described a one-way equation approach that numerically absorbs waves impinging on the boundaries. Mur (1981) described a finite-difference scheme, and Liao et al. (1984) described extrapolation of the wave fields in space and time using a backward difference polynomial. Another typical ABC is the perfectly matched layer (PML) in which layers of a material with both electric and magnetic loss (electric and magnetic conductivity) are introduced at the boundaries of the mesh to effectively suppress reflections and truncate the computational region (Taflove, 1995).

For example, Soontornpipit et al. (2004) discussed the design of a microstrip patch antenna for communication with medical implants. The FDTD method was used to evaluate the microstrip antenna design parameters. The edge of the cubic voxels was set to 1 mm, and Mur absorbing boundaries were placed 10 cells away from the antenna model. Kiourti et al. (2011, 2012, 2013; Kiourti and Nikita, 2012) conducted FDTD simulations to study the resonance and radiation performance of an implantable antenna operating in the medical implant communications service (MICS) band of 402–405 MHz for integration in wireless biotelemetry devices implanted in the human head. Free space surrounded the simulation set-ups by 200 mm, and Liao absorbing conditions were assumed at the boundaries to extend radiation infinitely far into space.

6.4 PHYSICAL MODELING

Numerical simulations do have some shortcomings. The computational time is usually very long, and it is generally not easy to simulate realistic conditions and include the effects of the surrounding environment. Measurements can be performed instead or as a means of validating the simulation results.

6.4.1 Physical Phantoms

In biomedical telemetry applications, experimental investigations can be performed with either real human subjects or physical phantoms. Physical phantoms are defined as surrogates of the human body that have electrical properties (relative permittivity and conductivity) equivalent to those of biological tissues.

Especially in safety testing where internal fields need to be measured, or in the case of wireless implants, measurements cannot be performed in human subjects by non-invasive methods, and physical phantoms become an essential tool. Furthermore, the use of phantoms can provide a stable and controllable EM environment, which cannot be easily realized with human subjects.

Tissue Material Formulation Physical phantoms consist of biological tissue-simulant materials, that is, materials in liquid, gel, or solid state that mimic the electrical properties of real biological tissue. Several recipes have been proposed to produce such materials accounting for different types of tissue. Furthermore, since it is not possible to produce a valid approximation for a wide frequency range by using a single formula, separate recipes are proposed for different operation frequency scenarios.

Liquid phantoms consist of an outer thin shell with very low RF absorption (usually made from fiberglass or other plastic material) that is further filled with a tissue-simulant liquid material. For frequencies in the range of 0.8–3 GHz, the relative permittivity of the outer shell should be less than 5, its loss tangent less than 0.05, and its thickness should be in the range of 2.0 $\pm$ 2 mm (Kanda et al., 2004). Liquid phantoms are very easy to prepare and their electrical properties are easily adjustable; most recipes are based on deionized water to which sugar and salt are added to adjust the relative permittivity and conductivity values, respectively.

Given their advantages, liquid phantoms have been widely used in the measurement of internal fields in safety studies, as well as in implantable antenna testing. For example, a liquid phantom made of water, sugar, salt and hydroxyethyl cellulose (HEC) (compound for adjusting the viscosity) was presented in Hartsgrove et al. (1987). A liquid UWB phantom material was developed in Hara and Kobayashi, (2005), and Liu et al. (2008) tested a skin tissue-implantable antenna immersed inside a skin-tissue-simulating fluid made of fruit sugar, salt, cellulose, and deionized water.

However, liquid phantoms suffer from the limited frequency range over which they have the desired electrical properties, the presence of the outer shell, their adequacy to simulate only high-water-content tissues, the instability of electrical properties (mainly due to water evaporation and growth of fungi), and the inaccuracy in human body modeling (since the internal structure is approximated as homogeneous).

Gel phantoms have the advantage of covering a wider frequency range than liquid phantoms, while they allow more accurate modeling of the human body by placing one on top of the other layers of gels mimicking different types of tissues. Similarly to liquid phantoms, they are very easy to prepare and their electrical properties are easily adjustable by appropriately adjusting the salt and sugar concentrations in the mixture.

Gel phantoms are formed by adding coagulants to the liquid solution. A common gelling agent is TX-150. Guy (1968) presented a recipe for a gel phantom composed of water, sodium chloride, TX-150, and polyethylene powder. Based on this recipe, Ito et al. (2001) developed a self-shaping phantom. Karacolak et al. (2008) added agarose (a linear polysaccharide) to a liquid mixture made of deionized water, sugar, and salt to fabricate skin-mimicking gels. The effects of sugar and salt on the relative permittivity and conductivity were further investigated, and it was found that the relative permittivity significantly decreases and conductivity slightly increases with increased sugar and salt concentration. Finally, Sani et al. (2010) added gelatin into liquid mixtures to convert them into gels and fabricate a three-layer phantom with layers representative of skin, fat, and muscle at 868 MHz.

However, similarly to liquid phantoms, gel phantoms are adequate only for high-water-content tissue modeling, and their electrical properties highly degrade over time (mainly due to water evaporation and growth of fungi).

Solid phantoms are made from materials that keep their shape over time, and they have the advantages of high accuracy in modeling the heterogeneous human body, fine mechanical stability, and minimized degradation over time (due to absence of water).

Several recipes have been proposed in the literature for solid phantoms. These include mixtures of Laminac 4110 (a polyester resin), acetylene black, and aluminum powder (Cheung and Koopman, 1976), flour, oil, and saline (Lagendijk and Nilsson, 1985), graphite powder and ceramic (Tamura et al., 1997), silicone rubber and carbon fiber (Nikawa et al., 1996), polyethyl methacrylate and carbon black (Chang et al., 2000), as well as agar, deionized water, polyethelene powder, sodium chloride, TX-151, and sodium dehydroacetate (Onishi et al., 2005). Solid phantoms are mainly used for analyzing propagation around the body; however, measurement of internal fields can also be performed by the method of thermography (Kobayashi et al., 1993).

On the other hand, fabrication of solid phantoms is generally more expensive and requires more complex and skilled production procedures as compared with liquid or gel phantoms.

Canonical Models Canonically shaped physical phantoms, that is phantoms with simplified geometries, have widely been used for biomedical telemetry applications in the literature, with special emphasis on the testing of tissue-implantable antennas.

Rectangular and cylindrical containers filled with skin- (Figure 6.9*a*) and muscle- (Figure 6.9*b*) tissue mimicking materials have been used to test prototypes of planar inverted-F and 3D spiral implantable antennas, respectively (Karacolak et al., 2009; Abadia et al., 2009). Karacolak et al. (2009) described the design and test of a miniature dual-band implantable antenna operating in the medical implant communications service (MICS) (402–405 MHz) and industrial, scientific, and medical

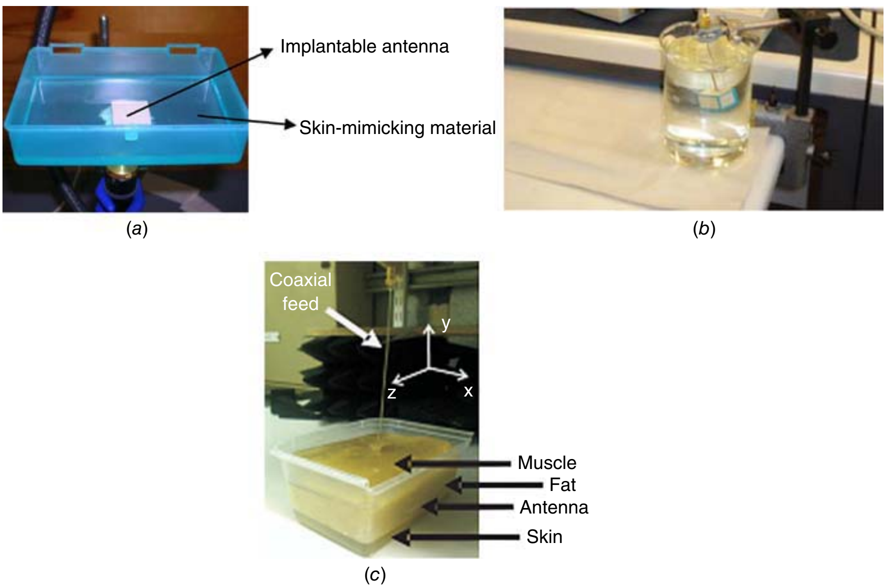

Figure 6.9 Canonical physical phantoms proposed in (*a*) Karacolak et al. (2009), (*b*) Abadia et al. (2009), and (*c*) Sani et al. (2010). (*See insert for color representation of the figure.*)

(ISM) (2.4–2.48 GHz) bands to be used in animal studies for medical research, while Abadia et al. (2009) presented the design and realization procedure of a MICS band 3D spiral radiator. Finally, a canonical three-layer phantom with layers representative of skin, fat, and muscle has been fabricated to investigate the radiation performance of an implantable antenna intended for RFID applications at 868 MHz (Figure 6.9*c*) (Sani et al., 2010).

Anatomical Models To provide realism in experimental modeling, several realistically shaped models have been developed that are filled with one or several different tissue-simulant liquids/gels to represent specific parts and tissues of the human body.

The most widely used homogeneous head phantom is the Specific Anthropomorphic Mannequin (SAM), which has been proposed by the Institute of Electrical and Electronics Engineers (IEEE, 2003) and the International Electrotechnical Commission (IEC, 2005) standards for compliance testing (Figure 6.10*a*). This phantom has also been adopted by the European Committee for Electrotechnical Standardization (CENELEC, 2001), the Association of Radio Industries and Businesses in Japan (ARIB, 2002), and the U.S. Federal Communications Commission (FCC, 1997). Prior to the introduction of the SAM phantom by the standardization bodies, the

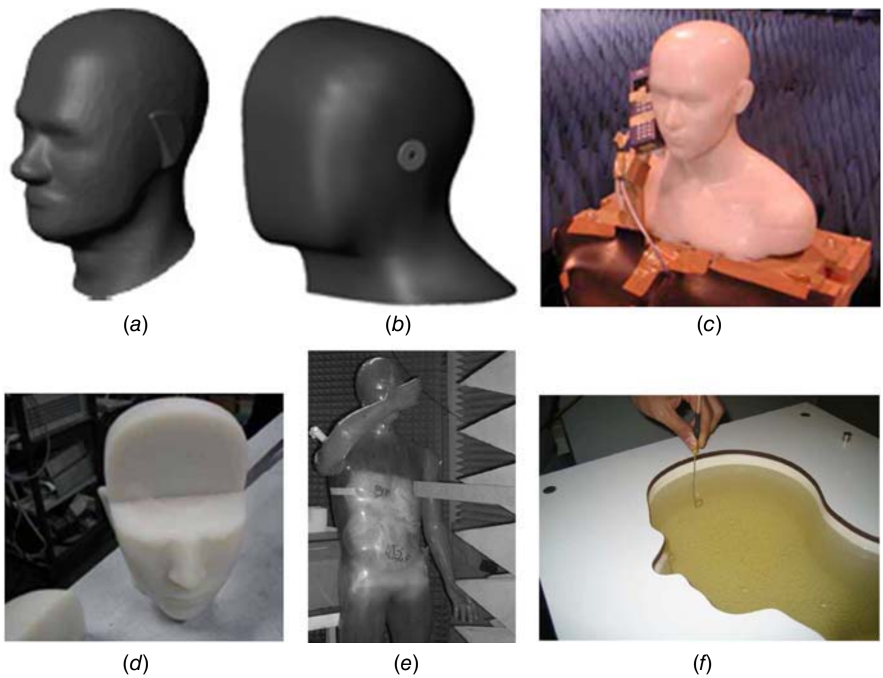

Figure 6.10 Anatomical physical phantoms proposed in (*a*) IEEE (2003) and IEC (2005), (*b*) FCC (2003), (*c*) Ito and Kawai (2004), (*d*) Ito and Kawai (2004), (*e*) Alomainy and Hao (2009), and (*f*) Chen et al. (2009).

Generic Twin Phantom was used, and several cellular phone models were authorized based on measurements with this phantom (Figure 6.10*b*) (FCC, 2003). Figure 6.10*c* shows a realistic-shaped upper-half body phantom for evaluating a future mobile satellite phone at 2.6 GHz, while Figure 6.10*d* shows the phantom for evaluation of the internal specific absorption rate (SAR) distribution (Ito and Kawai, 2004). A human phantom of approximately 1.7 m in height and 0.35 m in average width, with animal organs used to represent human tissues, has also been used as a radio propagation measurement setup (Alomainy and Hao, 2009) (Figure 6.10*e*). Finally, an anatomical head phantom filled with gray-matter-simulant liquid has been used to measure the transmission coefficient between implantable and exterior loop antennas (Chen et al., 2009) (Figure 6.10*f*).

6.4.2 Experimental Equipment and Measurements

Experimental investigations for biomedical telemetry applications mainly include measurements of:

1. The physical phantom's electrical properties (relative permittivity and conductivity)
2. The antennas' resonance characteristics (reflection coefficient frequency response, or, equivalently, resonance frequency and bandwidth)
3. Parameters that characterize propagation, transmission, and quality of communication (e.g., transmission coefficient, channel frequency response, etc.) in the wireless channel (formed between the medical device and monitoring/control equipment placed at a short distance)

Some of the most commonly applications used in the literature to perform such measurements are outlined below.

Measurement of Electrical Properties Even when tissue-simulant recipes are followed exactly, complex dielectric properties (or, equivalently relative permittivity and conductivity) of the fabricated material must be measured in order to ensure agreement with the intended theoretical values for the tissue to be modeled at the desired operation frequency.

Measurement and characterization of the relative permittivity and conductivity has attracted significant scientific interest not only in bioelectromagnetics but also in several other research and development fields including material science and microwave circuit design. Several measurement techniques have been developed [e.g., coaxial probe, slotted line, transverse electromagnetic (TEM) line, etc.] with each applying to specific materials, frequency ranges, and applications (Burdette et al., 1980; IEEE, 2001).

The most commonly used technique to measure the complex dielectric properties of physical phantoms is the open-ended coaxial probe technique, which is a broadband, nondestructive and noninvasive measurement method. This technique is based on the fact that the reflection coefficient of an open-ended coaxial probe

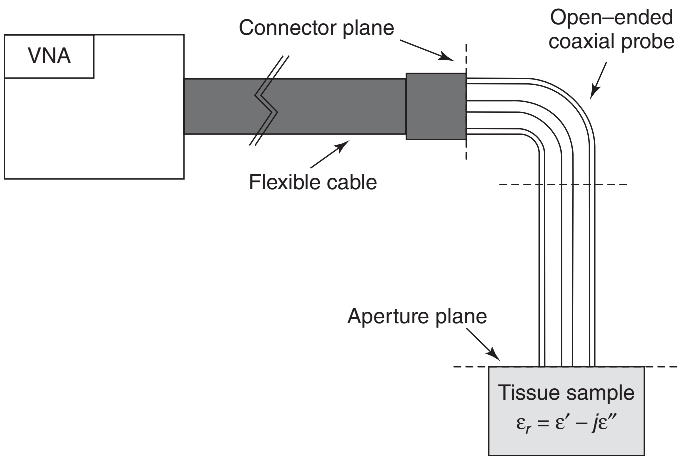

Figure 6.11 Open-ended coaxial probe technique for complex dielectric parameter measurement.

depends on the electrical parameters of the material that is attached to it. As shown in Figure 6.11, an open-ended coaxial probe attached to a vector network analyzer (VNA) is immersed into the liquid, or pressed against the solid specimen, and the reflection coefficient is measured. The VNA is calibrated at the probe aperture plane. Measured reflection coefficient values are subsequently postprocessed and converted into relative permittivity and conductivity values.

Calibration at the probe aperture plane can be performed in two ways:

- In the first way, reference liquids with known dielectric properties are used (e.g., water, saline, and methanol). The probe is directly calibrated at the aperture plane, by placing the short, open, and reference liquid standards at the end of the probe. This method is very direct and simple; however, it suffers from uncertainties in the selection and characterization of the reference liquids.
- In the second way, the VNA is initially calibrated at the connector plane by applying the short, open, and matched standards, and complex coefficient data referenced to the connector plane are recorded. A simulation (de-embedding) model of the open-ended probe is then used to compensate propagation in the probe and make the translation to the probe aperture. Measurement accuracy with this method highly depends on the physical characteristics of the probe's aperture. A rational function model (RFM) is finally applied at the probe aperture-referenced reflection coefficients to calculate the complex permittivity of the sample.

Recently, with the advance of new technologies, measurement of the complex dielectric parameters can easily be performed with commercially available dielectric probe kits. These consist of a VNA and an integrated software program to measure the complex reflection and transmission coefficients and directly convert them into electrical properties data. For example, Karacolak et al. (2008) performed dielectric constant and conductivity measurements of tissue-simulant gels using Agilent's 85070E dielectric probe kit and a network analyzer. The same technique was also used by the authors to measure the dielectric properties of 25 mm × 25 mm × 5 mm rat skin samples extracted from the middorsal area of rats (Karacolak et al., 2009). Samples were measured between 200 MHz and 20 GHz for 1800 frequency points, and 4 consecutive measurements were performed and averaged to ensure data reliability. The experimental set-ups are shown in Figure 6.12*a* and Figure 6.12*b*, respectively.

Measurement of Antenna Resonance Characteristics Impedance mismatch between an antenna and its feeding circuit causes reflection at the feed point of the antenna. Because of this reflection not all of the available power reaches the antenna, and thus the field strength of the radiated EM wave is reduced. The reflection coefficient (S_{11}) of an antenna describes this phenomenon and is defined as

$$S_{11} = \frac{Z_a - Z_0}{Z_a + Z_0} \tag{6.9}$$

where Z_a is the impedance of the antenna, and Z_0 is the impedance of the transmission feed line.

The reflection coefficient frequency response can easily be measured by means of a network analyzer. Before the measurements, the network analyzer should be calibrated for a suitable frequency range containing the operation frequency band of the antenna. To measure the reflection at the feed point of the antenna, a coaxial cable with an Sub-Miniature A (SMA) connector in one end is generally used. The cable is soldered to the feed point of the antenna, and the connector is connected to the

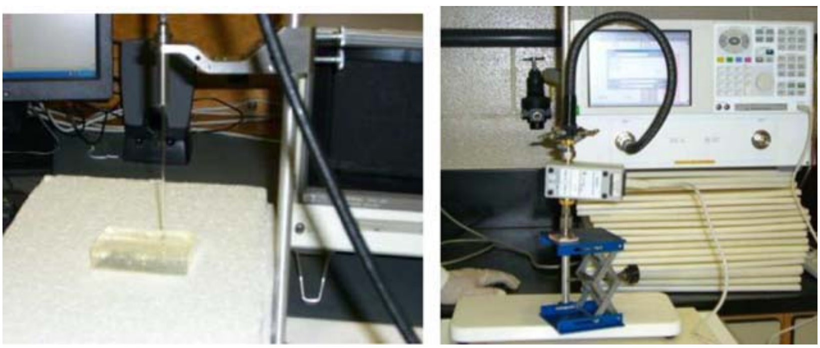

(*a*) (*b*)

Figure 6.12 Experimental setups for measuring the complex dielectric parameters of (*a*) skin-mimicking gels (Karacolak et al., 2008), and (*b*) rat skin samples (Karacolak et al., 2009) by means of a dielectric probe kit.

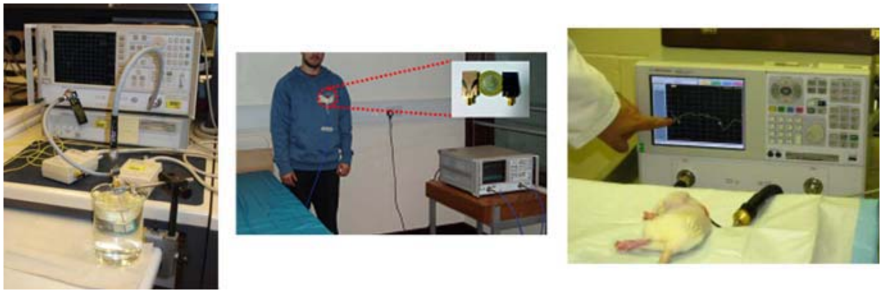

(*a*) (*b*) (*c*)

Figure 6.13 Experimental setups for measuring resonance characteristics of antennas (*a*) immersed in a tissue-simulant liquid (Abadia et al., 2009), (*b*) worn by a human subject (Alomainy et al., 2009), and (*c*) implanted inside a test animal (Karacolak et al., 2010).

network analyzer. In order to measure the reflection coefficient, the network analyzer transmits a small amount of power to the antenna and measures the reflected power.

For example, Abadia et al. (2009) built a prototype of their proposed muscle-implantable 3D spiral antenna and measured the magnitude of the reflection coefficient with a network analyzer (Figure 6.13*a*). A choke was used to reduce the current flow on the cable connecting to the network analyzer. Alomainy et al. (2009) measured UWB body-worn antennas placed directly on a tight cotton jumper worn by a human subject (Figure 6.13*b*). Finally, Karacolak et al. (2010) performed in vivo reflection coefficient measurements of implantable antennas using rats as model animals (Figure 6.13*c*). A stab wound allowed the coaxial cable attached to the antenna to exit the skin, and reflection coefficient measurements were performed immediately after the implantation surgery.

Specific Absorption Rate Measurements The dosimetric quantity most commonly used to determine the interaction of EM fields with human tissue is the specific absorption rate (SAR). The SAR represents power deposition in the body and is defined as

$$\mathrm{SAR} = \sigma \frac{|E|^2}{\rho} \tag{6.10}$$

where E is the root mean square (RMS) of the electric field (V/m), σ is the tissue conductivity (S/m), and ρ is the tissue density (kg/m^3). It is a measure of the power absorbed per unit mass of tissue and is expressed in watts per kilogram (W/kg).

The SAR can be experimentally measured by means of high-precision, multichannel exposition acquistion systems (EASY), as shown in Figure 6.14. Each measurement channel is characterized and processed individually, enabling high-precision isotropic measurements from lower MHz to above 10 GHz with a spatial resolution of a few millimeters. In the literature, there exists only a limited number of reported SAR measurements for biomedical telemetry systems. For example, Zhu and Langley (2009) performed SAR measurements for a dual-band textile wearable

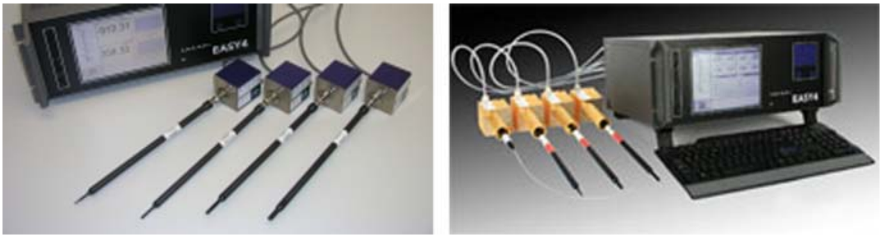

(*a*) (*b*)

Figure 6.14 (*a*) Portable four-channel exposure acquisition system and (*b*) portable four-channel exposure acquisition system hardened for use in hostile MRI environments up to 7 tesla.

antenna covering the 2.45-GHz and the 5-GHz wireless networking bands. Measured SAR values were found to be slightly higher than those of the simulations, which can be attributed to inaccuracies in phantom modeling and uncertainties in the realistic environment, as compared to that of the simulations (including the effects of connectors, cables, surrounding devices, and temperature).

Channel Measurements Several experimental investigations have been reported in the literature to assess propagation and transmission in wireless biomedical telemetry channels. Such channels are most commonly characterized by the transmission coefficient (S_{21}) between the antennas of the transmitter (biomedical telemetry device) and receiver (monitoring/control equipment placed at a short distance), which is defined so that

$$|S_{21}|^2 = \frac{P_r}{P_t} \tag{6.11}$$

where P_t is the power available at the transmitting port, and P_r is the power absorbed in a 50-Ω load terminating the receiving antenna.

Transmission coefficient measurements can be performed by connecting the transmitting and receiving antennas at the two ports of a VNA. The VNA measures the magnitude and phase of each frequency component of S_{21}, also known as the channel's frequency response. Such measurements often take place inside anechoic chambers, that is, chambers that are built from absorbers made of a high-quality, low-density lossy medium to provide a quiet zone needed to simulate the surrounding environment. Given the channel's frequency response, its time-domain response can subsequently be obtained by means of an inverse discrete fourier transform (IDFT), and time-domain channel characteristics (e.g., mean delay and RMS delay spread) can further be derived.

Several channel measurements have been reported in the literature for wearable, on-body antennas:

(a) UWB on-body propagation measurements have been performed in an anechoic chamber to characterize the channel between two pairs of different UWB antennas

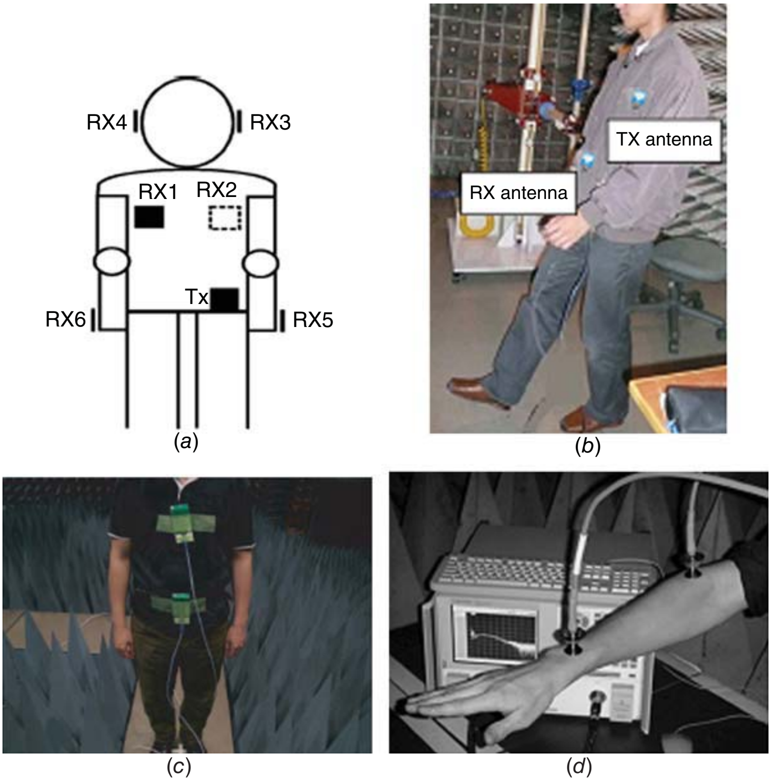

Figure 6.15 Channel measurement experimental setups found in (*a*) Alomainy et al. (2005), (*b*) Wang et al., (2009), (*c*) Takizawa et al. (2010), and (*d*) Lim et al. (2011).

[printed horn-shaped self-complementary antennas (HSCA) and planar inverted-cone antennas (PICA)] in terms of both frequency and time-domain response (Alomainy et al., 2005). Several positions between the transmitting (Tx) and receiving (Rx) antennas were investigated (Figure 6.15*a*).

(b) The chest-to-right-waist on-body link formed between two small-size, low-profile antennas mounted on the body has also been characterized (Wang et al., 2009). The transmitting and receiving antennas were fixed on the left side of the chest and the right side of the waist, respectively. The frequency-domain transfer function of the channel was measured in terms of a VNA and was further converted to the time domain by applying an IDFT. Measurements were conducted for 8 persons and 10 body postures per person, and the average delay profile of the channel was derived from the average of all 80 readings. Measurement antennas mounted on the body can be seen in Figure 6.15*b*.

(c) The performance of wearable wireless body area networks (WBANs) has been evaluated during walking motion (Takizawa et al., 2010). Received signal strength, packet error rate, and bit error rate were measured in an anechoic chamber and in an office room. Measurements were based on an Agilent Connected Solution using ADS Ptolemy. The signal waveform was calculated in the ADS Ptolemy installed in a laptop PC, and then the waveform was uploaded into a vector signal generator connected to a body-worn antenna. The receiving body-worn antenna received the transmitted signal, which was subsequently digitized at a spectrum analyzer and fed back to the ADS Ptolemy through ether cable (Figure 6.15*c*).

(d) Finally, propagation path loss measurements have been performed by considering two discone antennas attached to the arm of a volunteer (Lim et al., 2011). The transmitter was fixed on the wrist, while the receiver was positioned at different distances, as shown in Figure 6.15*d*. Antennas were connected to a calibrated VNA by two separate 50-Ω coaxial cables.

Channel measurements for ingestible and implantable biomedical telemetry systems have also been performed, as detailed below:

(a) The biotelemetric channel from ingestible implants has been measured by assuming a 4-cm-long monopole (without the ground plane) probe to be used as both the transmitting and receiving antennas (Figure 6.16*a*) (Alomainy and Hao, 2009). A near-field scanning system was used to obtain path loss data at different distances from the body.

(b) Transmission coefficient measurements have been conducted between an implantable antenna resting against a scalp phantom and a linearly polarized chip antenna used as a receiving (probing) antenna, by means of a full two-port calibrated VNA (Warty et al., 2008). A schematic of the experimental setup is shown in Figure 6.16*b*.

(c) Finally, measurements of $|S_{21}|$ in a mock biotelemetry link in porcine tissue have been performed to validate simulation results of a near-field biotelemetry link for an artificial hip joint. Both the implanted and external antennas were assumed to be stripped coax monopoles with a 3-cm-long exposed inner conductor (Weiss et al., 2009). The experimental setup is shown in Figure 6.16*c*.

6.5 SAFETY ISSUES

The biological effects of the emitted RF EM radiation can be divided into three categories: thermal, athermal, and nonthermal effects. Thermal effects cause tissue heating since the EM energy absorbed by the human tissues increases the molecular translational and rotational kinetic energy. In the case of athermal effects, even though the amount of absorbed EM energy is capable of heating the tissues, the temperature of the tissues does not increase because of the body thermoregulation mechanisms. Finally, non-thermal effects comprise complicated interactions between live cells and ions (calcium, potassium, etc.) and are related to the behavior of big molecules (proteins and DNA).

The effects of EM radiation in the human body depend not only on the field level but also on its operation frequency. Biomedical telemetry systems only produce nonionizing radiation. The photon energy of nonionizing radiation is low enough to break molecules and can only cause biological hazards in terms of thermal effects, that

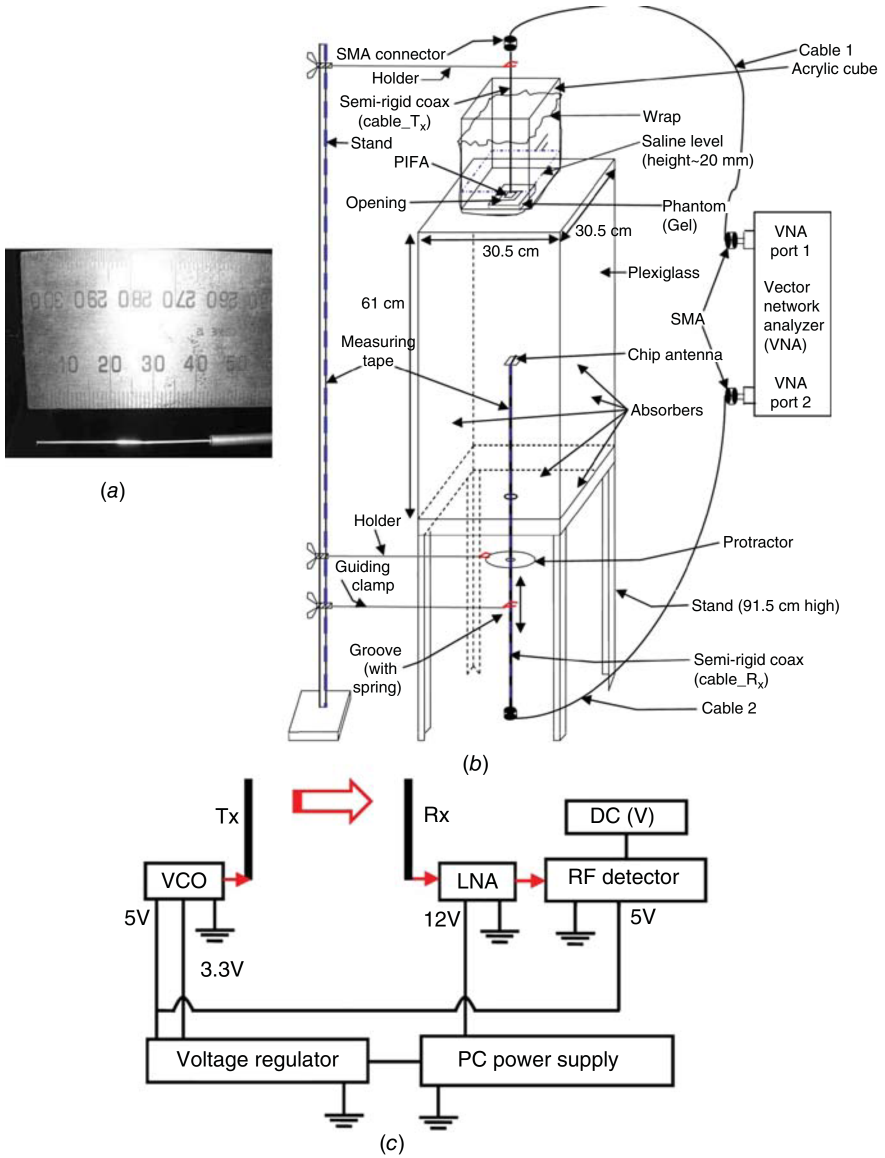

Figure 6.16 (*a*) Probe used as transmitter and receiver in the measurements of Alomainy and Hao (2009), and channel measurement experimental setups found in (b) Warty et al. (2008) and (*c*) Weiss et al. (2009).

is, tissue heating as energy of the photons is transformed into kinetic energy of the absorbing molecules. As EM waves propagate through the human body, their energy is absorbed by tissues and produces heating resulting from both ionic conduction and vibration of the dipole molecules of the water and the protein in tissue cells.

Dosimetry is necessary to "evaluate the dose" or, equivalently, to identify the dose metric that is closely related to the effect of concern. The proliferation of biomedical telemetry applications has given rise to national and international guidelines to determine exposure limits and ensure their safe use. Furthermore, considerable dosimetric research efforts have been devoted to assess the interactions between the EM radiation emitted by biomedical telemetry devices and the human body. These efforts have been motivated by three factors: (1) the need to evaluate potential health effects and compliance with standards (compliance testing), (2) the need to verify if existing protection standards are still adequate, and (3) the need to assess antenna performance and improve antenna design to minimize the energy absorbed in the human body while maximizing the radiated energy.

So far, all recommendations and regulations regarding the limits on allowable absorbed power in the body are based on quantitative short-term evaluation of the thermal effects caused by EM fields. The two major standards relating to RF radiation have been set up by the IEEE (1999, 2005) and the International Commission on Non-Ionizing Radiation Protection (ICNIRP, 1998), while several other standards exist as well [IEC, 2002; National Radiological Protection Board (NRPB), 2004; Health Protection Agency (HPA), 2008]. Countries can also set their own national standards, which are most commonly based on the guidelines set by international organizations.

Acceptable levels of radiation are typically expressed in terms of maximum permission exposures and SAR values averaged over specifically defined volumes of tissue. For example, by following the computational procedures recommended by IEEE, the average SAR is computed over 1-g (IEEE, 1999) or 10-g (IEEE, 2005) cubical volumes of voxels where no face of the averaging volume is external to the body. In cases where the cubical volume rule cannot be satisfied (e.g., at the surface of the body), special rules apply for setting the SAR value in a given voxel. On the contrary, the ICNIRP (1998) defines volumes of contiguous tissue, not necessarily in the shape of a cube.

Table 6.1 summarizes the most important SAR limits for uncontrolled exposure to mobile portable devices between 100 kHz and 6 GHz in the United States (IEEE, 1999, 2005) and Europe (ICNIRP, 1998). Uncontrolled environments are those where a person has no knowledge or control of his exposure (general public). Uncontrolled exposure is generally reduced by a factor of 5 from the controlled exposure. This happens because occupationally exposed population consists of adults who are trained to be aware of potential risks and to take appropriate precautions, while the general public comprises individuals of all ages and of varying health statuses, and may include particularly susceptible groups or individuals. A partial body average has been developed to deal with partial exposure to the sensitive head and eyes.

Finally, it is worth noting that new guidelines for limiting exposure to time-varying electric, magnetic, and electromagnetic fields have been developed to account for safety issues in the advanced biomedical telemetry technology of intrabody communications (currents propagating through the body). Table 6.2 summarizes ranges of threshold currents for the general public as set by the European Committee for Electrotechnical Standardization (ICNIRP, 2002). In general, it has been shown that

TABLE 6.1 IEEE and ICNIRP SAR Limits for Uncontrolled Exposure to Mobile Portable Devices between 100 kHz and 6 GHz

	IEEE C95.1-1999 (IEEE, 1999) (W/kg)	IEEE C95.1-2005 (IEEE, 2005) (W/kg)	ICNIRP (ICNIRP, 1998) (W/kg)
Whole-body average	0.08	0.08	0.08
Partial-body average	1.6	2	2
	Averaged over 1 g of tissue in the shape of a cube	Averaged over 10 g of tissue in the shape of a cube	Averaged over 10 g of contiguous tissue

TABLE 6.2 Ranges of Threshold Currents for General Public

	Threshold Current (mA)			
Effect	50/60 Hz	1 kHz	100 kHz	1 MHz
Touch perception	0.2–0.4	0.4–0.8	25–40	24–40
Pain on finger contact	0.9–1.8	1.6–3.3	33–55	28–50
Painful shock	8–16	12–24	112–224	
Severe shock	12–23	21–41	160–320	

Source: ICNIRP (2002).

threshold currents, which produce perception and pain, vary little over the frequency range of 100 kHz to 1 MHz, while they are unlikely to vary significantly over the frequency range up to about 110 MHz.

6.6 CONCLUSION

In this chapter, a summary was provided regarding the numerical and experimental techniques used to model and analyze EM wave propagation in biomedical telemetry systems. Canonical and anatomical models used for computational exposure assessment were presented, while phantoms used for experimental investigations were described. Safety issues were also addressed.

Analytical methods can be applied to simplified canonical geometries modeling the human body (or parts of it) and allow detailed calculation of the EM performance. However, numerical techniques implemented in computer codes running in powerful PCs prevail today to provide fast and accurate results, with the FDTD method dominating numerical modeling in bioelectromagnetics. Several anatomical models have been developed for subjects of varying age and ethnicity, with 1 mm resolution and higher being available in some cases.

In order to take into account the effects of the surrounding environment, or validate the simulation results, experimental investigations can also be performed. A range of liquid, gel, and solid canonical and anatomical physical phantoms have been developed for this purpose that account for specific types of tissue at given operation frequencies. Emphasis is most commonly given on measurements of electrical parameters, antenna reflection coefficient, and channel transmission coefficient, which can easily be performed by means of network analyzers and other commercially available equipment.

Finally, in order to ensure human safety, recommendations have been set by professional bodies and government agencies on the maximum allowable SAR levels. However, the health hazards occurring from long-term exposure to these new technologies are far from settled. All organizations agree that with any new technology it is a sensible precautionary approach to keep the situation under ongoing review.

REFERENCES

Abadia J, Merli F, Zurcher JF, Mosig JR, Skrivervik AK. 2009. 3D-spiral small antenna design and realization for biomedical telemetry in the MICS band. *Radioengineering*, 18(4):359–367.

Abd-Alhameed RA, Excell PS, Mangoud MA. 2005. Computation of specific absorption rate in the human body due to base-station antennas using a hybrid formulation. *IEEE Trans. Electromag. Compat.*, 47:374–381.

Ackerman MJ. 1998. The visible human project. *Proc IEEE*, 86(3):504–511.

Alomainy A, Hao Y. 2009. Modeling and characterization of biotelemetric radio channel from ingested implants considering organ contents. *IEEE Trans. Antennas Propag.*, 57(4):999–1005.

Alomainy A, Hao Y, Parini CG, Hall PS. 2005. Comparison between two different antennas for UWB on-body propagation measurements. *IEEE Antennas Wireless Propag. Lett.*, 4:31–34.

Alomainy A, Sani A, Rahman A, Santas JG, Hao Y. 2009. Transient characteristics of wear able antennas and radio propagation channels for ultrawideband body-centric wireless communications. *IEEE Trans. Antennas Propag.*, 57(4):875–884.

Association of Radio Industries and Businesses in Japan (ARIB). 2002. Specific Absorption Rate (SAR) Estimation for Cellular Phone, ARIB STD-T56.

Bao JZ, Lu ST, Hurt WD. 1997. Complex dielectric measurements and analysis of brain tissues in the radio and microwave frequencies. *IEEE Trans. Microw. Theory Tech.*, 45(10):1730–1741.

Burdette E, Cain F, Seals J. 1980. In vivo probe measurement technique for determining dielectric properties at VHF through microwave frequencies. *IEEE Trans. Microw. Theory Tech.*, 8 (4):414–427.

Campbell AM, Land DV. 1992. Dielectric properties of female human breast tissue measured in vitro at 3.2 GHz. *Phys. Med. Biol.*, 37:193–210.

Cavagnaro M, Pisa S. 1996. Simulation of cellular phone antennas by using inductive lumped elements in the 3D-FDTD Algorithm. *Microw. Opt. Technol. Lett*. 13(6):324–326.

Chang JT, et al. 2000. A conductive plastic for simulating biological tissue at microwave frequencies. *IEEE Trans. Electromagn. Compat*., 42:76–81.

Chen J, Feng Z, Jin JM. 1998. Numerical simulation of SAR and B1-field inhomogeneity of shielded RF coils loaded with the human head. *IEEE Trans. Biomed. Eng.*, 45:650–659.

Chen ZN, Liu GC, See TSP. 2009. Transmission of RF signals between MICS loop antennas in free space and implanted in the human head. *IEEE Trans. Antennas Propag*., 57(6):1850–1853.

Cheung AY, Koopman DW. 1976. Experimental development of simulated biomaterialsfor dosimetry studies of hazardous microwave radiation. *IEEE Trans. Microw. Theory Tech.*, 24:669–673.

Christopoulos C. 1995. *The Transmission Line Modeling Method: TLM*. Piscataway, NJ, IEEE Press.

Chuang H, Chen W. 1997. Computer simulation of the human-body effects on a circular loop-wire antenna for radio-pager communications at 152, 280, and 400 MHz. *IEEE Trans. Vehicular Tech*., 46(3):544–559.

Curto S, Ammann MJ. 2007. Electromagnetic coupling mechanism in a layered human tissue model as reference for 434 MHz RF medical therapy applicators. Proc. IEEE Antennas and Propag. Soc. Int. Symp., Honolulu, pp. 3185–3188.

Dimbylow PJ. 2002. Fine resolution calculations of SAR in the human body for frequencies up to 3 GHz. *Phys. Med. Biol*., 47:2835–2846.

Engquist B, Majda A. 1977. Absorbing boundary conditions for the numerical simulation of waves. *Proc. Natl. Acad. Sci*., 74:1765–1766.

European Committee for Electrotechnical Standardization (CENELEC). 2001. Basic Standard for the Measurement of Specific Absorption Rate Related to Exposure to Electromagnetic Fields from Mobile Phones (300 MHz–3 GHz), EN 50361.

Federal Communications Commission (FCC). 1997. Federal Communications Commission (FCC) evaluating compliance with FCC guidelines for human exposure to radio frequency electromagnetic fields. Supplement C to *OET Bulletin 65* (Edition 9701), Washington, DC.

Federal Communications Commission (FCC). 2003. Equipment authorization system generic search. Available http://gullfoss2.fcc.gov/prod/oet/cf/eas/reports/GenericSearch.cfm.

Gabriel C, Gabriel S, Corthout E. 1996. The dielectric properties of biological tissues. *Phys. Med. Biol*., 41:2231–2293.

Gandhi OP, Lazzi G, Furse CM. 1996. Electromagnetic absorption in the human head and neck for mobile telephones at 835 and 1900 MHz. *IEEE Trans. Microw. Theory Tech*. 44:1884–1897.

Gupta A, Abhayapala TD. 2008. Body area networks: Radio channel modelling and propagation characteristics. Australian Communications Theory Workshop, pp. 58–63.

Guy A. 1968. Analyses of electromagnetic fields induced in biological tissues by thermographic studies on equivalent phantom models. *IEEE Trans. Microw. Theory Tech.*, 19(2):205–214.

Hafner C. 1990. *The Generalized Multipole Technique for Computational Electromagnetic*. Boston: Artech House.

Hara D, Kobayashi T. 2005. Development of ultra wideband electromagnetic phantom materials for antennas and propagation studies. 13th Conf. Microw. Tech., pp. 64–67.

Harrington R. 1968. *Field Computation by Moment Method*. New York: Macmillan.

Hartsgrove G, Kraszewski A, Surowiec A. 1987. Simulated biological materials for electromagnetic radiation absorption studies. *Bioelectromagnetics*, 8: 29–36.

Health Protection Agency (HPA) 2008. *Protection of Patients and Volunteers Undergoing MRI Procedures*. Chilton: Health Protection Agency.

International Electrotechnical Commission (IEC). 2005. *IEC Standard 62209-1. Human Exposure to Radio Frequency Fields from Hand-Held and Body-Mounted Wireless Communication Devices–Human Models, Instrumentations, and Procedures*. IEC.

Institute of Electrical and Electronics Engineers (IEEE). 1999. C95.1-1999 IEEE Standard for Safety Levels with respect to Human Exposure to Radio Frequency Electromagnetic Fields, 3 kHz to 300 GHz. New York: IEEE.

Institute of Electrical and Electronics Engineers (IEEE). 2001. Draft: Recommended practice for determining the spatial-peak specific absorption rate (SAR) in the human body due to wireless communications devices: experimental techniques, p. 1528.

Institute of Electrical and Electronics Engineers (IEEE) Standard 1528 SCC34. 2003. IEEE recommended practice for determining the peak spatial-average specific absorption rate (SAR) in the human head from wireless communications devices: measurement techniques.

Institute of Electrical and Electronics Engineers (IEEE). 2005. C95.1-2005 IEEE Standard for Safety Levels with respect to Human Exposure to Radio Frequency Electromagnetic Fields, 3 kHz to 300 GHz. New York: IEEE.

International Commission on Non-Ionising Radiation Protection (ICNIRP). 1998. Guidelines for limiting exposure to time-varying electric, magnetic, and electromagnetic fields (up to 300 GHz). *Health Phys.* 74:494–522.

International Commission on Non-Ionizing Radiation Protection (ICNIRP). 2002. Guidelines for limiting exposure to time-varying electric, magnetic, and electromagnetic fields (up to 300 GHz), 513.

International Electrotechnical Commission (IEC). 2002. *Medical Electrical Equipment: Part 2. Particular Requirements for the Safety of Magnetic Resonance Equipment for Medical Diagnosis*. Geneva: IEC.

Ito K, Furuya K, Okano Y, Hamada L. 2001. Development and characteristics of a biological tissue-equivalent phantom for microwaves. *Electron Commun. in Japan* (Part I: Communications), 84(4).

Ito K, Ida I, Wu M. 1992. Body effect on characteristics of small loop antenna in pager systems. *IEEE Antennas Propag. Society Int. Symp*., pp. 1081–1084.

Ito K, Kawai H. 2004. Phantoms for evaluation of interactions between antennas and human body. URSI EMTS International Symposium, pp. 1104–1106.

Kanda M, Ballen M, Salins S, Chou C, Balzano Q. 2004. Formulation and characterization of tissue equivalent liquids used for RF densitometry and dosimetry measurements. *IEEE Trans. Microw. Theory Tech*., 52(8):2046–2056.

Karacolak T, Cooper R, Butler J, Fisher S, Topsakal E. 2010. In vivo verification of implantable antennas using rats as model animals. *IEEE Antennas Propag. Lett.*, 9(10):334–337.

Karacolak T, Cooper R, Topsakal E. 2009. Electrical properties of rat skin and design of implantable antennas for medical wireless telemetry. *IEEE Trans. Antennas Propag*., 57(9):2806–2812.

Karacolak T, Hood AZ, Topsakal E. 2008. Design of a dual-band implantable antenna and development of skin mimicking gels for continuous glucose monitoring. *IEEE Trans. Microw. Theory Techn*., 56(4):1001–1008.

Kim J, Rahmat-Samii Y. 2004. Implanted antennas inside a human body: Simulations, designs, and characterizations. *IEEE Trans. Microw. Theory Tech.*, 52(8):1934–1943.

Kiourti A, Christopoulou M, Nikita KS. 2011. Performance of a novel miniature antenna implanted in the human head for wireless biotelemetry. *IEEE APS Int. Symp. Antennas Propag.*, pp. 392–395.

Kiourti A, Costa JR, Fernandes CA, Santiago AG, Nikita KS. 2012. Miniature implantable antennas for biomedical telemetry: From simulation to realization. *IEEE Trans. Biomed. Eng.*, 59(11):3140–3147.

Kiourti A, Nikita KS. 2012. Miniature scalp-implantable antennas for telemetry in the MICS and ISM bands: design, safety considerations and link budget analysis. *IEEE Trans. Antennas Propag.*, 60(6):3568–3575.

Kiourti A, Nikita KS. 2013. Numerical assessment of the performance of a scalp-implantable antenna: Effects of head anatomy and dielectric parameters. *Wiley Bioelectrom.*, 34(3):167–179.

Kiourti A, Psathas KA, Costa JR, Fernandes CA, Nikita KS 2013. Dual-band implantable antennas for medical telemetry: A fast design methodology and validation for intracranial pressure monitoring. *Prog. Electrom. Res.*, 141:161–183.

Kobayashi T, Nojima T, Yamada K, Uebayashi S. 1993. Dry phantom composed of ceramics and its application to SAR estimation. *IEEE Trans. Microw. Theory Tech.*, 41(1):136–140.

Koulouridis S, Nikita KS. 2004. Study of the coupling between human heads and cellular phone helical antennas. *IEEE Trans. Electromagn. Compat*. 46:62–70.

Kuhn A, Keller T. 2006. The influence of capacitive properties on nerve activation in transcutaneous electrical stimulation. Proc. Int. Symp. Comput. Methods Biomech. Biomed. Eng., p. 7.

Kuhn S, Cabot E, Christ A, Capstick M, Kuster N. 2009. Assessment of the radio-frequency electromagnetic fields induced in the human body from mobile phones used with hands-free kits. *Phys. Med. Biol.*, 54:5493–5508.

Lagendijk JJW, Nilsson P. 1985. Hyperthermia dough: A fat and bone equivalent phantom to test microwave/radiofrequency hyperthermia heating systems. *Phys. Med. Biol.*, 30:709–712.

Lazebnik M, et al. 2007. A large-scale study of the ultrawideband microwave dielectric properties of normal breast tissue obtained from reduction surgeries. *Phys. Med. Biol.*, 52:2637–2656.

Liao Z P, Wong H L, Yang B, Yuan Y. 1984. A transmitting boundary for transient wave analysis. *Sci. Sin. A*, 27:1063–1076.

Lim HB, Baumann D, Li EP. 2011. A human body model for efficient numerical characterization of UWB signal propagation in wireless body area networks. *IEEE Trans. Biomed. Eng.*, 58(3):689–697.

Lin JC. 1976. Electromagnetic pulse interaction with mammalian cranial structures. *IEEE Trans. Biomed. Eng*. 23:61–65.

Liu WC, Chen SH, Wu, CM. 2008. Implantable broadband circular stacked PIFA antenna for biotelemetry communication. *J. Electromagn. Waves Appl.*, 22:1791–1800.

Meyer FJC, et al. 2003. Human exposure assessment in the near field of GSM base-station antennas using a hybrid finite element/method of moments technique. *IEEE Trans. Biomed. Eng.*, 50(2):224–233.

Monk P, Suli E. 1994. Error estimates for yee's method on non-uniform grids. *IEEE Trans. Magn.*, 30:3200–3203.

Mur G. 1981. Absorbing boundary conditions for the finite-difference approximation of the time-domain electromagnetic-field equations. *IEEE Trans. Electromag. Compat.*, 23:377–382.

Nagaoka T, Watanabe S, Sakurai K, Kunieda E, Watanabe W, Taki M, Yamanaka Y. 2004. Development of realistic high-resolution whole-body voxel models of Japanese adult males and females of average height and weight, and application of models to radio-frequency electromagnetic-field dosimetry. *Phys. Med. Biol.*, 49(4):1–15.

National Radiological Protection Board (NRPB). 2004. Advice on limiting exposure to electromagnetic fields (0–300 GHz). Doc. NRPB 15, 1–35.

Nikawa Y, Chino M, Kikuchi K. 1996. Soft and dry phantom modeling material using silicone rubber withcarbon fiber. *IEEE Trans. Microw. Theory Tech.*, 44(10):1949–1953.

Nikita KS, Cavagnaro M, Bernardi P, Uzunoglu NK, Pisa S, Piuzzi E, Sahalos JN, Krikelas GI, Vaul JA, Excell PS, Cerri G, Chiarandini S, De Leo R, Russo P. 2000. A study of uncertainties in modeling antenna performance and power absorption in the head of a cellular phone user. *IEEE Trans. Microw. Theory Tech.* 48:2676–2685.

Onishi T, Ishido R, Takimoto T. 2005. Biological tissue-equivalent agar-based solid phantoms and SAR estimation using the thermographic method in the range of 3–6 GHz. *IEICE Trans. Commun.*, E88-B(9):3733–3741.

O'Rourke APO, Lazebnik M, Bertram JM, Converse MC, Hagness SC, Webster JG, Mahvi DM. 2007. Dielectric properties of human normal, malignant and cirrhotic liver tissue: in vivo and ex vivo measurements from 0.5 to 20 GHz using a precision open-ended coaxial probe. *Phys. Med. Biol.*, 52:4707–4719.

Peyman A, Gabriel C, Grant EH, Vermeeren G, Martens L. 2009. Variation of the dielectric properties of tissues with age: The effect on the values of SAR in children when exposed to walkie-talkie devices. *Phys. Med. Biol.* 54:227–241.

Peyman A, Holden SJ, Watts S, Perrott R, Gabriel C. 2007. Dielectric properties of porcine brain tissue in the transition from life to death at frequencies from 800 to 1900 MHz. *Phys. Med. Biol.*, 52:2229–2245.

Peyman A, Rezazadeh A, Gabriel C. 2001. Changes in the dielectric properties of rat tissue as a function of age at microwave frequencies. *Phys. Med. Biol.*, 46:1617–1629.

Psychoudakis D, Lee G, Chen C, Volakis J. 2008. Body-worn diversity antennas for squad area networks (SAN). URSI General Assembly.

Renhart W, et al. 1994. Modeling and calculation of influences of RF-fields on the human body using the finite element method. *IEEE Trans. Mag.*, 30(5):3092–3095.

Sani A, Rajab M, Foster R, Hao Y. 2010. Antennas and propagation of implanted RFIDs for pervasive healthcare applications. *Proc IEEE*, 98(9):1648–1655.

Schmid G, Neubauner G, Udo MI, Francois A. 2003. Dielectric properties of porcine brain tissue in the transition from life to death at frequencies from 800 to 1900 MHz. *Bioelectromagnetics*, 24:413–422.

Schwan HP, Li K. 1956. Hazards due to total body irradiation by radar. *Proc. IRE*, 44:1572–1581

Silvester P, Ferrari R. 1996. *Finite Elements for Electrical Engineers*. Cambridge University Press.

Smith SR, Foster KR. 1985. Dielectric properties of low-water-content tissues. *Phys. Med. Biol.*, 30:965–973.

Soontornpipit P, Furse CM, Chung YC. 2004. Design of implantable microstrip antenna for communication with medical implants. *IEEE Trans. Microw. Theory Tech.*, 32(8):1944–1951.

Sullivan D. 1990. Three-dimensional computer simulation in deep regional hyperthermia using the finite-difference time-domain method. *IEEE Trans. Microw. Theory Tech.*, 38:204–211.

Sullivan DM, Borup DT, Gandhi OP. 1987. Use of the finite-difference time-domain method in calculating EM absorption in human tissues. *IEEE Trans. Biomed. Eng.*, 34:148–157.

Taflove A. 1995. *Computational Electrodynamics*. London: Artech House.

Taflove A, Hagness S. 2000. *Computational Electrodynamics: The Finite Difference Time Domain Method*. London: Artech House.

Takizawa K, Watanabe K, Kumazawa M, Hamada Y, Ikegami T, Hamaguchi K. 2010. Performance evaluation of wearable wireless body area networks during walking motions in 444.5 MHz and 2450 MHz. 32nd Annu Int Conf IEEE EMBS, pp. 370–373.

Tamura H, Ishikawa Y, Kobayashi T, Nojima T. 1997. A dry phantom material composed of ceramic and graphite powder. *IEEE Trans. Electromagn. Compat.*, 39(2):132–137.

Traille A, Yang L, Rida A, Tentzeris M. 2008. A novel liquid antenna for wearable bio-monitoring applications. *IEEE MTT-S*, 923–926.

Wang Q, Tayamachi T, Kimura I, Wang J. 2009. An on-body channel model for UWB body area communications for various postures. *IEEE J. Sel. Areas Commun.*, 57(4):991–998.

Warty R, Tofighi MR, Kawoos U, Rosen A. 2008. Characterization of implantable antennas for intracranial pressure monitoring: Reflection by and transmission through a scalp phantom. *IEEE Trans. Microw. Theory Tech.*, 56(10):2366–2376.

Wegmueller MS, Kuhn A, Froehlich J, Oberle M, Felber N, Kuster N, Fichtner W. 2007. An attempt to model the human body as a communication channel. *IEEE Trans. Biomed. Eng.*, 54(10):1851–1857.

Weil CM. 1975. Absorption characteristics of multilayered sphere models exposed to UHF/microwave radiation. *IEEE Trans. Biomed. Eng.*, 6:468–476.

Weiss MD, Smith JL, Bach J. 2009. RF coupling in a 433-MHz biotelemetry system for an artificial hip. *IEEE Antennas Wireless Propag. Lett.*, 8:916–919.

Wiart J, Hadjem A, Gadi N, Bloch I, Wong MF, Pradier A, Lautru D, Hanna VF, Dale C. 2005. Modeling of RF head exposure in children. *Bioelectromagnetics* 26:S19–S30.

Wiart J, Hadjem A, Wong M, Bloch I. 2008. Analysis of RF exposure in the head tissues of children and adults. *Phys. Med. Biol.* 53:3681–3695.

Yee KS. 1966. Numerical solution of initial boundary value problems involving Maxwell' s equations in isotropic media. *IEEE Trans. Antennas Propag.*, 14(3):302–307.

Zhao Y, Hao Y, Alomainy A, Parini C. 2006. UWB on-body radio channel modeling using ray theory and subband FDTD method. *IEEE Trans. Microw. Theory Tech.*, 54(4):1827–1835.

Zhou H, Oosterom van A. 1992. Computation of the potential distribution in a four-layer anisotropic concentric spherical volume conductor. *IEEE Trans. Biomed. Eng.*, 39:154–158.

Zhu S, Langley R. 2009. Dual-band wearable textile antenna on an EBG substrate. *IEEE Trans. Antennas Propag.* 57(4):926–935.

Zubal IG, Harrell CR, Smith EO, Rattner Z, Gindi G, Hoffer PB. 1994. Computerized three-dimensional segmented human anatomy. *Med. Phys.* 21(2):299–302.